Aerosol activation characteristics and prediction at the central European ACTRIS research station Melpitz, Germany

Yuan Wang[1,2,3*], Silvia Henning[1*], Laurent Poulain[1], Chunsong Lu[2], Frank Stratmann[1], Yuying Wang[2], Shengjie Niu[2,4], Mira L. Pöhlker[1], Hartmut Herrmann[1], and Alfred Wiedensohler[1]

1. Leibniz Institute for Tropospheric Research (TROPOS), 04318 Leipzig, Germany.

2. Collaborative Innovation Center on Forecast and Evaluation of Meteorological Disasters, Nanjing University of Information Science and Technology, 210044 Nanjing, China.

3. Collaborative Innovation Center for Western Ecological Safety, Lanzhou University, 730000 Lanzhou, China.

4. College of Safety Science and Engineering, Nanjing Tech University, 210009 Nanjing, China.

*Correspondence: Yuan Wang (wang_yuan@lzu.edu.cn) and Silvia Henning (henning@tropos.de)

Abstract: Understanding aerosol particle activation is essential for evaluating aerosol indirect effects (AIEs) on climate. Long-term measurements of aerosol particle activation help to understand the AIEs and narrow down the uncertainties of AIEs simulation. However, they are still scarce. In this study, more than 4-year aerosol comprehensive measurements were utilized at the central European research station Melpitz, Germany, to gain insight into the aerosol particle activation and provide recommendations on improving the prediction of number concentration of cloud condensation nuclei (CCN, N_{CCN}). (1) The overall CCN activation characteristics at Melpitz is provided. As supersaturation (SS) increases from 0.1% to 0.7%, the median N_{CCN} increases from 399 to 2144 cm^{-3}, which represents 10% to 48% of the total particle number concentration with a diameter range of 10 – 800 nm, while the median hygroscopicity factor (κ) and critical diameter (D_c) decrease from 0.27 to 0.19 and from

176 to 54 nm, respectively. (2) Aerosol particle activation is highly variable across seasons, especially at low SS conditions. At $SS = 0.1\%$, the median N_{CCN} and activation ratio (AR) in winter are 1.6 and 2.3 times higher than the summer values, respectively. (3) Both κ and the mixing state are size dependent. As the particle diameter (D_p) increases, κ increases at D_p of ~40 to 100 nm and almost stays constant at D_p of 100 to 200 nm, whereas the degree of the external mixture keeps decreasing at D_p of ~40 to 200 nm. The relationships of κ vs. D_p and degree of mixing vs. D_p were both fitted well by a power-law function. (4) Size-resolved κ improves the N_{CCN} prediction. We recommend applying the κ - D_p power-law fit for N_{CCN} prediction at Melpitz, which performs better than using the constant κ of 0.3 and the κ derived from particle chemical compositions and much better than using the N_{CCN} (AR) vs. SS relationships. The κ - D_p power-law fit measured at Melpitz could be applied to predict N_{CCN} for other rural regions. For the purpose of improving the prediction of N_{CCN}, long-term monodisperse CCN measurements are still needed to obtain the κ - D_p relationships for different regions and their seasonal variations.

1. Introduction

The specific subset of aerosol particles that serves as nuclei for the condensation of water vapor, forming cloud droplets at a given supersaturation (SS) condition, is known as cloud condensation nuclei (CCN). Aerosol particle activation affects the aerosol and cloud interactions (ACI), thereby changing the cloud microstructure (Zhao et al., 2012; Jia et al., 2019; Wang et al., 2019), precipitation (Khain, 2009; Wang et al., 2011; Fan et al., 2012, 2018), radiation (Twomey, 1974, 1977; Albrecht, 1989; Zhao and Garrett, 2015), and by these effects the global climate (Ramanathan et al., 2001;

Rosenfeld et al., 2019). The latest sixth assessment report from IPCC (2021) pointed out that aerosol indirect effects (AIEs) remain the most considerable uncertainty in assessing the anthropogenic contribution to present and future climate change.

The ambient SS and aerosol activation ability are both important for predicting the number concentration of cloud droplets. The classical Köhler theory (Köhler, 1936), combining the Raoult law with the Kelvin effect, illustrates that the aerosol particle activation depends on particle size, chemical composition, and the given SS. Petters and Kreidenweis (2007) parameterized the Raoult term with a single hygroscopicity factor κ to capture the water activity without needing to know anything about the dissolved compounds. Different perspectives have been presented on the influence of particle size and composition on the CCN activation. In terms of a single aerosol particle, the actual particle size plays a more important role than the chemical composition for activation because of the different range in which κ and particle diameter (D_p) vary and the reciprocal relationship between κ and the third power of the critical D_p (D_c^3) at a given SS. As for a population of aerosol particles, Dusek et al. (2006) concluded that particle number size distribution (PNSD) matters more than the chemical composition distribution, which has been supported by many experiments. Even sometimes, assuming a constant κ still predicted CCN number concentration (N_{CCN}) well (e.g., Sihto et al., 2011; Wang et al., 2018a). Andreae and Rosenfeld (2008) reviewed the previous studies on aerosol particle activation and recommended that for modeling purposes, the global κ values of 0.3±0.1 and 0.7±0.2 can be representative for continental and marine aerosol, respectively, which has been widely used to predict N_{CCN}. The regional variability should be emphasized because the mean κ measured in urban, rural, and forest exhibits significant differences. For instance, Sihto et al. (2011) suggested an average κ of 0.18 to predict the CCN activation well in boreal forest conditions in

74   Hyytiälä, Finland. A fixed κ of 0.31 suffices to calculate the N_{CCN} in a suburban site

75   located in the center of the North China Plain (Wang et al., 2018a). The mean κ is 0.5

76   in a near-coast background station (CESAR Tower) in Netherlands (Schmale et al.,

77   2018). The median κ ranges from 0.02 to 0.16 at $SS = 0.1-1.0\%$ in an urban background

78   site in Budapest, Hungary (Salma et al., 2021). Therefore, the assumption of a constant

79     $\kappa = 0.3$ may not be appropriate when trying to predict N_{CCN} for different continental

80   regions.

81   Additionally, some experiments, especially conducted on more diverse particulate

82   sources, have indicated chemistry does play an important role in N_{CCN} variability (e.g.,

83   Nenes et al., 2002; Petters and Kreidenweis, 2007; Rose et al., 2010). Not only the bulk

84   chemical composition with a constant κ should be considered for N_{CCN} prediction, but

85   the size-resolved chemical composition (Deng et al., 2011; Wu et al., 2016) and the

86   mixing state should be applied (Su et al., 2010; Zhang et al., 2014). Information on the

87   organic aerosol fraction improves N_{CCN} prediction considerably (Poulain et al., 2010;

88   Zhang et al., 2016; Kuang et al., 2020). Freshly formed particles are about 1 nm in

89   diameter (Kulmala et al., 2012), which must grow to tens of nanometers in diameter to

90   serve as the effective CCN at a relatively high SS of ~1% (Dusek et al., 2006) and even

91   larger than 200 nm to be efficient at SS less than 0.1% (Deng et al., 2013). Aerosol

92   chemical composition changes during the growing and aging processes. For instance, κ

93   increases with particle size caused by photochemical processes which enhancing

94   secondary inorganic species formation and going along with an increase in particle size

95   (Massling et al., 2009; Zhang et al., 2017; Wang et al., 2018b). On the other hand, in

96   sulfate dominated new particle formation (NPF) events with subsequent particle growth

97   by condensation of organic vapors, the κ of small particles may exceed the κ of the

98   larger ones (Wang et al., 2018a). If the κ of organic aerosol increases from 0.05 to 0.15,

the global average aerosol radiative forcing would decrease by ~1 W m^{-2}, which is in the same order of magnitude as the overall climate forcing of anthropogenic aerosol during the industrialization period (Rastak et al., 2017).

To obtain the regional parameters of aerosol particle activation, extensive field campaigns have been conducted worldwide. Besides the significant difference in spatial, also the temporal variations of aerosol activation characteristics are essential for N_{CCN} prediction (Andreae and Rosenfeld, 2008). Most of the observations lasted 1–2 months or even less, mainly focusing on the effects of short-term weather processes or pollution events on aerosol particle activation, such as the effects of the summer monsoon (Jayachandran et al., 2020), wet removal (Croft et al., 2009), NPF events (Dusek et al., 2010; Wu et al., 2015), biomass burning (Rose et al., 2010), and aerosol particle aging as well as oxidation processes (Zhang et al., 2016, 2017). The long-term CCN measurements (of at least one full year) are still rarely reported, resulting in insufficient knowledge concerning the seasonal and annual cycles of aerosol particle activation, which are also critical for model predictions and evaluations. Burkart et al. (2011) reported the particle activation in the urban background aerosol of Vienna, Austria, based on 11-month aerosol and CCN concentration measurements. Paramonov et al. (2015) reported a synthesis of CCN measurements within the EUCAARI network using the long-term data collected at 14 locations. Pöhlker et al. (2016) presented the climatology of CCN properties of a remote central Amazonian rain forest site using 1-year measurements. Che et al. (2017) provided the aerosol-activation properties in the Yangtze River Delta, China, based on ~1-year measurements. Using the long-term (of most > 1 year) aerosol and CCN concentration measurements from 12 sites, Schmale et al. (2018) presented the spatial differences in aerosol particle activation for various regional backgrounds. However, systematic studies focusing on the seasonal cycle of

size-resolved particle activation and respective CCN predictions are still scarce in the central European continent. Such a study would be of great help for understanding ACI and narrowing down the regional uncertainties in climate predictions.

In this investigation, more than 4-year comprehensive measurements of aerosol physical, chemical, and activation properties collected at the ACTRIS (Aerosol, Clouds and Trace Gases Research Infrastructure, http://www.actris.eu/) site Melpitz, Germany, are utilized. The major objective is to gain insight into the aerosol particle activation and provide recommendations on methods for N_{CCN} predictions. We present therefore the long-term observations and seasonal cycles of various particle activation variables such as N_{CCN}, activation ratio, critical diameter, size-resolved κ and mixing state. Furthermore, we evaluated the accuracy of N_{CCN} calculated from five different activation schemes and finally provide recommendations on N_{CCN} predictions at Melpitz and for other rural regions.

2. Methodology

2.1 Experiment details

Atmospheric aerosol measurements were conducted at the Melpitz observatory (51.54°N, 12.93°E, 86 m above sea level), 50 km to the northeast of Leipzig, Germany. The aerosol particles observed at Melpitz can be regarded as representative for the central European rural background conditions (Birmili et al., 2009). The surroundings of the site are mostly pastures and forests without significant sources of anthropogenic emissions. More detailed descriptions of the Melpitz site can be found, for example, in Poulain et al. (2020).

This study focuses on the physicochemical properties and the activation ability of aerosol particles using the data collected at Melpitz from August 2012 to October 2016. Figure 1 depicts the experimental setup. All instruments were in the same container

laboratory and utilized the same air inlet. Ambient aerosol particles were first pretreated

through a PM_{10} Anderson inlet and an automatic aerosol diffusion dryer kept the relative

humidity in sampling lines less than 40% following the ACTRIS recommendations.

Subsequently, the aerosol flow was divided into the different instruments using an

isokinetic splitter. Particle number size distributions (PNSD) were measured using a

Dual-mobility particle size spectrometer (D-MPSS, TROPOS-type; Birmili et al., 1999;

Wiedensohler et al., 2012) with a diameter range of 5 – 800 nm. An aerosol chemical

speciation monitor (ACSM, Aerodyne Inc; Ng et al., 2011) was used to measure the

chemical compositions of the non-refractory submicron aerosol particulate matter

(nitrate, sulfate, chloride, ammonium, and organics). A multi-angle absorption

photometer (MAAP, model 5012, Thermo Scientific; Petzold and Schönlinner, 2004)

was used to measure the particle light absorption coefficients and to estimate the

equivalent black carbon (eBC) mass concentration. For simultaneous measurement of

particle and CCN number size distributions, dried aerosol particles were passed through

the bipolar charger to establish charge equilibrium (Wiedensohler, 1988) and then

through a differential mobility analyzer (DMA) for selecting a monodisperse particle

fraction. After the DMA, the flow was split to pass through a condensation particle

counter (CPC, model 3010, TSI) to measure the total number concentration of the

selected monodisperse condensation nuclei (N_{CN}) and through a cloud condensation

nuclei counter (CCNC, model 100, Droplet Measurement Technologies; Roberts and

Nenes, 2005) to measure the N_{CCN}. Thus, the size dependent activated fraction (AF,

N_{CCN}/N_{CN}) curve, i.e., the AF at a certain diameter (D_p) of dry particles, could be

obtained. The losses in both instruments were checked and it was corrected for in the

inversion routine. The coupling between size selection and CCNC was programmed in

a way that the size resolved measurements started only after the temperature and

thereby the *SS* of the CCNC was stabilized. As the diameter scan started after *SS* stabilization, the measurement itself was the same length at all *SS* conditions. At fully stabilized CCNC conditions we did one D_p scan at per *SS* setting. A total of five different *SS* conditions was set in the CCNC instrument (0.1%, 0.2%, 0.3%, 0.5%, and 0.7%). A complete *SS* cycle lasted ~2.5 hours and the slight variations in the 2.5h total *SS* cycle was only due to the waiting time until the temperature of the CCNC was stabilized.

All the instrumentation was frequently calibrated within the framework of the European Center for Aerosol Calibration (ECAC, https://www.actris-ecac.eu/). The ACSM was regularly calibrated according to the manufacturer's recommendations with 350 nm monodispersed ammonium nitrate and ammonium sulfate particles (Freney et al., 2019). The D-MPSS was calibrated following the recommendations in Wiedensohler et al. (2018). Throughout the campaign, the CCNC was calibrated once a year following the procedures outlined in Rose et al. (2008) with using the E-AIM model (Clegg et al. 1998). The measurement uncertainties of these instruments should be noted. The uncertainty in the MAAP is within 10% (Müller et al., 2011), and those in the D-MPSS and CCNC are both on the order of 10% (Wiedensohler et al., 2018; Rose et al., 2008). For the *SS* setting in CCNC, Gysel and Stratmann (2013) pointed out that an achievable accuracy in *SS* is 10 % (relative) at *SS* > 0.2%, and less than 0.02 % (absolute) at the lower *SS*. For the ACSM data, the uncertainty in determining the total non-refractory mass is 9%. While for the individual chemical components, the uncertainty is 15% for nitrate, 28% for sulfate, 36% for ammonium, and 19% for organic matter (Crenn et al., 2015).

Due to instrument failures and maintenance operations, missing measurements occurred during the campaign. Effective data coverage is shown in Figure S1 in supporting information (SI). Overall, the CCNC, D-MPSS, and ACSM-MAAP

captured 45578 AF curves, 103052 PNSDs, and 26876-hour aerosol chemical measurements, which covered 63%, 92%, and 77% of the campaign time, respectively. For 42% of the time all these instruments were measuring together.

2.2 Methods

Each AF curve (N_{CCN}/N_{CN} vs. D_p) was first corrected for multiply charged particles. Multiply (mostly doubly) charged particles appear in the AF curve as a plateau or shoulder at small diameters because they have the same electrical mobility diameter as singly charged smaller particles (Rose et al., 2008; Henning et al., 2014). To correct for this, the fraction of multiple charged particles as determined from the D-MPSS measurements was subtracted from each value of N_{CCN}/N_{CN} in AF. The PNSD from the D-MPSS measurements (5 to 800 nm) are needed as the DMA-CCNC size range does not cover the large particle fraction, which is essential for the correction. Subsequently, we obtained the corrected AF curves.

Each corrected AF curve was fitted with a sigmoid function,

$$AF = a + b / \left(1 + \exp\left(-\frac{D_p - D_c}{\sigma_s} \right) \right) \qquad (1)$$

Where a is the offset from 0 in the y direction and b is the height of the upper plateau of the sigmoidal function, D_c is the critical diameter, and σ_s is a measure for the width of the sigmoid function. This AF fit was multiplied with the PNSD to gain the CCN number size distribution and by integrating the total number of CCN, i.e., N_{CCN}.

The critical diameter (D_c) of dry particles, κ, and mixing state at each SS condition can be derived from the AF fit results. Affected by aerosol mixing, the AF rises gradually from 0 to the max (~1) rather than displaying an intermittent mutation. D_c is defined as the diameter of the dry particles from which 50% of the particles are activated at the given SS.

The shape of the AF curve, i.e., the relative width of the AF, represents the degree of external mixture, which can be quantified by the ratio of $(D_{75} - D_{25})/D_c$ (Jurányi et al., 2013). D_{75} and D_{25} are the diameters at which 75% and 25% of the particles are activated at the given *SS*. Internal mixture implies that all particles with any given dry size have equal κ with $(D_{75} - D_{25})/D_c = 0$, whereas a distribution of different κ at a given particle size can be observed for externally mixed aerosol with higher $(D_{75} - D_{25})/D_c$ values. Note that the particle composition varying at different sizes is not defined as external mixing in this study. Jurányi et al. (2013) confirmed the reliability of this approach by comparing the κ distributions derived from parallel monodisperse CCN measurements and HTDMA measurements.

According to the derivation of κ-Köhler theory (Petters and Kreidenweis, 2007), the κ can be calculated from D_c at a given *SS*:

$$\kappa = \frac{4A^3}{27D_c{}^3 \ln^2(1 + SS/100)} \tag{2a}$$

with

$$A = \frac{4\sigma_{s/a}M_w}{RT\rho_w} \tag{2b}$$

where $\sigma_{s/a}$ is the droplet surface tension (assumed to be that of pure water, $0.0728\ \mathrm{Nm^{-2}}$), M_w the molecular weight of water, R the universal gas constant, T the absolute temperature, ρ_w the density of water, and A can be considered a function of T. Thus, the size-resolved κ (pair of κ and D_c) can be obtained at each *SS* cycle. Our monodisperse CCN measurements provide the size-resolved κ within D_p (D_c) of ~40−200 nm, which depends largely on the *SS* setting of 0.1% to 0.7%. Note that equation 2a is derived from an approximation of κ-Köhler equation and when κ is less than 0.2, it causes a slight bias in calculating κ (Petters and Kreidenweis, 2007). Additionally, the debate about

243   the importance of $\sigma_{s/a}$ changes and the connected bulk/surface partitioning on activation

244   of aerosols is on ongoing (e.g., Ovadnevaite et al., 2017; Vepsäläinen et al., 2022),

245   which is not focused on in this study.

246   Besides deriving it from the monodisperse CCN measurements, κ can be derived

247   from the ACSM and MAAP chemical composition measurements (κ_{chem}) using the

248   Zdanovskii–Stokes–Robinson (ZSR) mixing rule (Zdanovskii, 1948; Stokes and

249   Robinson, 1966) combined with κ-Köhler theory:

$$\kappa_{chem} = \sum_i \varepsilon_i \kappa_i \tag{3}$$

250   where κ_i and ε_i mean the κ and volume fraction for each component, respectively, and

251   i is the number of the component in the mixture. The ε_i was derived from its measured

252   component i mass concentration and density (ρ_i). A simple ion-pairing scheme (Gysel

253   et al., 2007) was used in this study with the κ_i and ρ_i values listed in Table 1 (Wu et al.,

254   2015). A κ of 0.1 is used for particulate organics (Dusek et al., 2010; Gunthe et al., 2009,

255   2011). For black carbon, we use a κ of 0 (Rose et al., 2011; Schmale et al., 2018).

256   The CCN number size distribution is a part of the particle number size distribution

257   (PNSD), which approximately corresponds to the part of PNSD with $D_p > D_c$ when

258   assuming particles to be internally mixed (Figure S2 in SI). The assumption of the

259   internal mixing could be reasonable because the median values of the parameter b and

260      $(D_{75} - D_{25})/D_c$ are 1.0 and 0.18. Thus, D_c plays a critical role on diagnosing N_{CCN} in

261   models, which can be derived from κ parameterization at a given SS. When κ is obtained,

262      $D_c(\kappa, SS)$ is calculated from equation 2a. And, assuming an internal mixture, the

263   predicted N_{CCN} is the integration of the PNSD from D_c, that is,

$$Predicted\ N_{CCN} = \int_{D_c}^{800} PNSD(D_p) dD_p \tag{4}$$

3. Results

3.1 Aerosol activation characteristics

As SS increases, the CCN number size distribution broadens towards smaller particle sizes (Figure S3 in SI), causing an increase in N_{CCN} and activation ratio (AR, i.e., ratio of N_{CCN} to total aerosol number concentration with a diameter range of 10 to 800 nm, N_{aero}). At Melpitz, the median N_{CCN} and AR increase from 399 to 2144 cm^{-3} and 0.10 to 0.48 when SS increases from 0.1% to 0.7%. As shown in Figure 2, the N_{CCN} measured at Melpitz is slightly higher than that measured in more remote rural background stations, e.g., in Vavihill, Sweden (Fors et al., 2011), Hyytiälä, Finland (Paramonov et al., 2015), Southern Great Plains, USA (Liu and Li, 2014), Mahabaleshwar, India (Singla et al., 2017). However, compared to the N_{CCN} measured in polluted regions (e.g., Rose et al., 2010; Deng et al., 2011; Kim et al., 2014; Varghese et al., 2016), the Melpitz N_{CCN} is much lower.

Figure 3a presents the N_{CCN} vs. SS and AR vs. SS relationships at each season and all datasets at Melpitz. The two relationships are similar, and both can be fitted well with using a power-law function (Twomey, 1959). The fit was also performed with an error function (Pöhlker et al., 2018) and the fitted parameters are in SI (Table S2). Over the whole period, the median values of the slope parameter and the coefficient in the N_{CCN}-SS power-law fit are 2851 cm^{-3} and 0.75, respectively, which are within the range of values for continental aerosol (slope parameter of 600–3500 cm^{-3} and coefficient of 0.4–0.9) reported in Seinfeld and Pandis (2016). The slope parameters in the power-law fitting represent the sensitivity of the N_{CCN} and AR to the variation in SS, which are highest in summer and lowest in winter. The seasonal variations of N_{CCN} and AR at SS = 0.1% and 0.7% are shown in Figure 3b. In summer, the median N_{CCN} and AR are both lowest at SS = 0.1%, which contributed to the largest sensitivity of N_{CCN} and AR to SS,

289   i.e., the largest slope parameter in the power-law fitting among the four seasons.

290   Additionally, the shape of the PNSD contributed to explain the sensitivity of N_{CCN} and

291   AR to SS. The PNSD in summer was steepest in the 40-200 nm size range among the

292   four seasons (Figure S4 in SI). Thus, in summer, a small shift in D_c will change the

293   N_{CCN} and AR much more than those in winter where the PNSD looks broader, causing

294   the strong sensitivity of N_{CCN} and AR to SS.

295   To explain the seasonal variations in aerosol activation characteristics, we

296   investigated the PNSD and chemical compositions as shown in Figure 4. In summer,

297   affected by the frequent NPF events (Ma et al., 2015; Wang et al., 2017), the Aitken-

298   mode particles with $D_p < 100$ nm accounted for the largest portion of the PNSD (Figure

299   S4 in SI), resulting in the highest N_{aero} and the smallest geometric mean diameter

300   ($GMD = \exp\left(\frac{\Sigma_i\, n_i \times ln D_i}{N_{aero}}\right)$)) among the four seasons. Additionally, in summer, there was

301   the lowest bulk κ_{chem} with median value of 0.24 corresponding to the highest organic

302   mass fraction (56% of total mass), which could be related to the strong formation of the

303   secondary organic aerosol (SOA). Therefore, the N_{CCN} and AR both kept relatively low

304   values in summer, especially at low SS conditions (e.g., at $SS = 0.1\%$). On the contrary

305   in winter, the relatively low number concentration of Aitken-mode particles caused the

306   lowest N_{aero} and the largest GMD among the four seasons, which could be owing to the

307   rare NPF events. Meanwhile, in winter, low temperatures favored the particulate phase

308   of nitrate (Poulain et al., 2011), causing the highest nitrate mass fraction (31% of total

309   mass) among the four seasons, which might explain the highest κ_{chem} (median value of

310   0.34). Taking all three together, the lowest N_{aero}, the largest GMD, as well as the highest

311   κ_{chem}, contribute to the highest AR value in winter at each SS condition. The

312   relationships between κ_{chem} and each particle component, and the correlations among

313   seasonal median values of N_{aero}, GMD, and κ_{chem} are in SI (Text S1, Figures S5 and S6).

314   Additionally, no significant yearly trends of the CCN activation characteristics are

315   found during the 4-year measurements and the results are provided in SI (Text S2 and

316   Figure S7).

3.2 Size-resolved particle hygroscopicity factor and mixing state

318   The hygroscopicity factor and the mixing state directly influence the D_c and the

319   shape of the AF curve, thereby changing the N_{CCN} at a given SS condition. Affected by

320   the variations of particle composition, these two parameters are not constant and both

321   vary with particle size and season.

322   Figure 5a shows monthly median values of κ_{chem} and κ calculated from

323   monodisperse CCN measurements (κ_{CCN}) at SS of 0.1% and 0.7%. Their seasonal

324   median values are summarized in Table 2. At Melpitz, the median κ_{CCN} decreased from

325   0.27 to 0.19 as SS increased from 0.1% to 0.7%, which was less than the median

326   bulk κ_{chem} of 0.3. The seasonal variation of κ_{CCN} at SS of 0.1% is similar to that of κ_{chem},

327   whereas the seasonal trend in κ_{CCN} is much weaker at SS = 0.7%. Essentially, the

328   relationship between κ_{CCN} and SS is determined by the κ_{CCN} vs. D_p relationship. The

329   κ_{CCN} at SS of 0.1% and 0.7% correspond to the median D_c (i.e., D_p) of 176 and 54 nm,

330   respectively. As the ACSM is sensitive to particle mass rather than number

331   concentration, the bulk composition is dominated by the contribution of the larger

332   particles. In the median volume size distribution of particle, the peak diameter was at

333   ~300 nm (Poulain et al., 2020). Thus, κ_{chem} may be representative for the larger particles

334   rather than for the smaller particles. Owing to the positive correlation between κ and

335   D_p (Figure 6a), the κ_{chem} representing for the larger particles could be greater than the

336   κ_{CCN} for the smaller particles. Figure 5b depicts the monthly variation of D_c at SS of

337   0.1% and 0.7%, which shows the opposite trend to $\kappa_{CCN}(SS)$ because of the negative

correlation of $D_c{}^3(SS)$ vs. $\kappa(SS)$ shown in equation 2a. Compared to the D_c at lower SS

conditions (e.g., 0.1%), D_c has a more significant seasonal trend at higher SS conditions

(e.g., 0.7%). At $SS = 0.7\%$, the low κ_{CCN} caused the large D_c in summer, whereas the

high κ_{CCN} caused the small D_c in spring and winter.

The monthly trend of the external-mixing degree ($(D_{75} - D_{25})/D_c$) is shown in

Figure 5c. Jurányi et al. (2013) pointed out that the $(D_{75} - D_{25})/D_c$ ranged from 0.08 to

0.12 for ammonium sulfate calibration measurements at $SS = 0.1-1.0\%$, which

indicated an internal mixture within measurement accuracy. For our measurements, the

median $(D_{75} - D_{25})/D_c$ over all datasets range from 0.15 to 0.20 at $SS = 0.1-0.7\%$. The

median $(D_{75} - D_{25})/D_c$ was low in summer and spring and high in winter and autumn.

The results tend to indicate that the aerosol particles at Melpitz were more internally

mixed in summer and spring whereas less internally mixed in winter and autumn. In

summer, the less contribution from anthropogenic emissions and the faster aging

process as well as SOA formation caused by atmospheric chemistry certainly contribute

to make particles more internally mixed. Changes in organic aerosol (OA) composition

can be found in Crippa et al. (2014), Poulain et al. (2014), and Chen et al. (2022). In

cold seasons, the local pollution (100 km around) is dominated by liquid fuel, biomass,

and coal combustions mostly for house heating (van Pinxteren et al., 2016). During

winter long-range transport from the eastern wind bring to the station continental air

masses which are strongly influence by anthropogenic emissions (in opposition to

western marine air masses). These particles are a mixture of different anthropogenic

sources emitted all along the transport as well as including some local and regional

sources (most house heating). All of them at different aging state cause the overall

particles more externally mixed.

As mentioned above, κ_{CCN} (and $(D_{75} - D_{25})/D_c$) vs. D_p relationships determine the

relationship between κ_{CCN} (and $(D_{75} - D_{25})/D_c$) and SS. Monodisperse CCN

measurements provide the size-resolved κ and $(D_{75} - D_{25})/D_c$. At a given SS condition,

κ_{CCN} represents the κ of particles at $D_p = D_c$, and the same is true for $(D_{75} - D_{25})/D_c$. As

shown in Figure 6a, κ_{CCN} increases with D_p at D_p range of ~40 to 100 nm, whereas κ_{CCN}

almost stays constant at D_p of 100 to 200 nm for all seasons. Additionally, the increase

κ_{CCN} with D_p varies with season. The κ_{CCN} vs. D_p relationship is fitted by a power-law

function at each season. In summer, there is the lowest slope parameter in the κ_{CCN} vs.

D_p power-law fit, meaning that the κ_{CCN} is least sensitive to D_p. Compared to the cold

seasons, the anthropogenic emissions linked to house heating strongly reduce in

summer which affects the smaller particles, and the dominant small particles ($D_p < 100$

nm) are associated to NPF and the SOA formation. NPF is a complex process which

depends on the availability of condensing material (H_2SO_4 and organic), as well as pre-

existing particles (coagulation and condensation sink parameters). Therefore, same

condensing material on the gas phase can either condense on pre-existing particles

(usually larger than 100 nm and then detected by ACSM) or lead to NPF formation. A

direct consequence of it is a probable smaller effect of the size dependent chemical

composition of the particles. This might explain why κ_{CCN} at SS of 0.1% and 0.7 % are

closer, i.e., the weaker sensitive of κ_{CCN} to D_p in summer. Figure 6b presents the $(D_{75} -$

$D_{25})/D_c$ vs. D_p relationship. As particle size increases, $(D_{75} - D_{25})/D_c$ decreases at D_p of

~40 to 200 nm for all seasons, meaning that small particles are less internally mixed.

The reason is that during the aerosol aging process, not only particle size increases but κ

becomes more uniform. The $(D_{75} - D_{25})/D_c$ vs. D_p relationship is also fitted well by a

power-law function at each season. The lowest absolute value of the slope parameter

was observed in summer, indicating that the degree of external mixture was least

sensitive to D_p, which could be related to the less mixing between the local emissions

388   and long-range transport particles in summer.

3.3 N_{CCN} prediction at Melpitz

390   N_{CCN} plays an important role in modeling the formation and evolution of clouds.

391   In this section, we evaluate the accuracy of N_{CCN} predicted from five schemes. Table 3

392   introduces the five schemes, which can be summarized into two categories. From

393   polydisperse CCN measurements, the N_{CCN} (AR) and *SS* relationships can be obtained,

394   and their fitting results can be used to predict N_{CCN} at the given *SS* conditions, which

395   belongs to the 1st category, corresponding to the N1 and N2 schemes in Table 3,

396   respectively. Compared to CCN measurements, it is generally more common and

397   simpler to obtain the PNSD measurements. Thus, we usually predict N_{CCN} using the

398   real-time PNSD combined with the parameterized $\kappa(D_c)$, which belongs to the 2nd

399   category. The 2nd category includes the last three schemes (K1, K2, and K3) in Table 3,

400   but they vary in assuming κ. The K1 scheme used a fixed κ of 0.3 without temporal and

401   size-dependent variations, as recommended for continental aerosol (Andreae and

402   Rosenfeld., 2008), which is also the median value of κ_{chem} over all data setting at

403   Melpitz. The K2 scheme used the bulk κ_{chem} calculated from aerosol chemical

404   composition, which is also non-size-dependent but changes over time. The K3 scheme

405   used the κ - D_p power-law fit results shown in Figure 6a, which are size-dependent

406   without temporal variations at each season. Applying the κ - D_p power-law equation

407   into equation 2a, D_c can be derived as function of *SS*,

$$D_c = \left(\frac{4 \times A^3}{27 \times coef \times \ln^2(1 + SS/100)} \right)^{\frac{1}{slope+3}} \tag{5}$$

408   where the *slope* and *coef* represent the slope parameter and the coefficient in κ - D_p

409   power-law fit. Subsequently, the predicted N_{CCN} can be calculated through equation 4.

410   The 2nd category assumed that aerosol particles are internally mixed at a particular D_p,

411   as used in many previous N_{CCN} prediction studies (e.g., Deng et al., 2013; Pöhlker et al.,

412   2016; Wang et al., 2018a).

413   The prediction results are shown in Figure 7. The linear equation (y = kx) is used

414   to fit the relationship between the predicted N_{CCN} and the measured one, and its slope

415   represents the mean ratio of the predicted N_{CCN} to the measured N_{CCN}. The relative

416   deviation (RD) equals the ratio of the absolute difference between the predicted N_{CCN}

417   and the measured one to the measured N_{CCN},

$$RD = \frac{|predicted\ N_{CCN} - measured\ N_{CCN}|}{measured\ N_{CCN}}. \tag{6}$$

418   The median RD was used to quantify the deviation between predictions and

419   measurements of each scheme. The slope and median RD shown in Figure 7 are both

420   calculated from all five SS conditions for each season. As shown in Figure 7, the N1

421   and N2 schemes only provide rough estimates of the N_{CCN} which is reflected in the high

422   median RD. The results for N1 and N2 schemes are similar in that they both predict the

423   overall mean N_{CCN} well (slopes of approximately 1.0) but with large median RDs.

424   Compared to N1 scheme, the N2 scheme is better because of the lower median RD.

425   Compared to the 1st category (the N1 and N2 schemes), the 2nd category (the K1, K2,

426   and K3 schemes) predicts N_{CCN} better because of the lower median RD. The results for

427   K1 and K2 are similar in that they both overestimate N_{CCN} by approximately 10%

428   (slopes of approximately 1.1) with similar median RDs. The reason for the N_{CCN}

429   overestimation is that the constant κ of 0.3 and the real-time bulk κ_{chem} are both greater

430   than the κ_{CCN} at each season. In winter, the κ_{CCN} was highest and the difference between

431   the κ_{CCN} and the parameterized κ in K1 and K2 scheme was lowest, causing the best

432   prediction of N_{CCN} among the four seasons. Owing to the largest difference between the

433   κ_{CCN} and the parameterized κ, the N_{CCN} prediction was worst in summer for K1 scheme

434 and in autumn for K2 scheme. The K3 scheme appears to be the best one for N_{CCN}

435 prediction among the five schemes which is reflected in the lowest median RDs and the

436 fit slope of ~1.0 for different seasons. The evaluations of the five schemes for the N_{CCN}

437 prediction at each SS condition and each season are provided in Figure S8 in SI.

438   The K3 scheme provides an improved prediction of N_{CCN}, which is obvious when

439 compared to N1 and N2 schemes. Compared to K1 and K2 schemes, the K3 scheme

440 reduced approximately 10% overestimation of N_{CCN} because the fitting slope decreased

441 ~0.1 on average. We simply evaluate the effects of the 10% overestimation in N_{CCN} on

442 predictions of cloud radiative forcing and precipitation. The methods are in Text S3 in

443 SI and Wang et al. (2019). Essentially, an overestimation of N_{CCN} leads to overestimate

444 the number concentration of cloud droplet (N_C) in models. Theoretically, it can reduce

445 3.2% overestimation of cloud optical thickness, corresponding to global average

446 difference of 1.28 Wm^{-2} when assuming the cloud shortwave cooling effect of 40 Wm^{-2}

447 ^{2} (Lee et al., 1997), which amounts to approximately one-third of the direct radiative

448 forcing from a doubling CO_2. Additionally, the overestimation in N_{CCN} (and N_C) leads

449 to underestimate the strength of the autoconversion process in cloud (Liu et al., 2006),

450 thereby suppressing precipitation. Therefore, although ACSM measurements can derive

451 κ_{chem} and thus predict N_{CCN}, the monodisperse CCN measurements are still important

452 to obtain the κ - D_p relationship and thus improve the predictions of N_{CCN} (and N_C) and

453 climate.

454   Figure 8 compared the κ - D_p relationship measured at different regions. The κ -

455 D_p relationship measured at Melpitz is similar to that measured at other rural regions

456 with similar κ - D_p power-law fitting results, e.g., the Vavihill station in Sweden (Fors

457 et al., 2011) and the Xinken station in China (Eichler et al., 2008). Therefore, the κ - D_p

458 power-law fit measured at Melpitz could be applied to predict N_{CCN} for these rural

459   regions. We conducted a CCN closure test to support this conclusion. Due to lacking

460   the data of PNSD and CCN measurements at Vavihill and Xinken stations, we applied

461   the κ - D_p power-law fitting measured at the two rural stations (green and purple lines

462   in Figure 8) to predict the N_{CCN} at Melpitz. Good prediction results were obtained with

463   mean deviations of ~1% (Figure S9 in SI). However, it may cause considerable

464   deviations for different aerosol background regions, e.g., the suburb stations in Xingtai,

465   China (Wang et al., 2018a), Xinzhou, China (Chen et al., 2022), and Paris, France

466   (Mazoyer et al., 2019), the coast of Barbados (Kristensen et al., 2016), the amazon

467   rainforest (Pöhlker et al., 2016), and the urban stations in Budapest, Hungary (Salma et

468   al., 2021), Guangzhou, China (Chen et al., 2022), and Shanghai, China (Ye et al., 2013),

469   because their κ - D_p relationships are different from that measured at Melpitz.

4. Conclusions

471   Aerosol particle activation plays an important role in determining N_C, thereby

472   affecting cloud microphysics, precipitation processes, radiation, and climate. To reduce

473   the uncertainties and gain more confidence in the simulations on AIEs, long-term

474   measurements of aerosol activation characteristics are essential. However, they are still

475   rarely reported. Based on more than 4-year comprehensive measurements conducted at

476   the central European ACTRIS site Melpitz, Germany, this study presents a systematic

477   seasonal analysis of aerosol activation characteristics and N_{CCN} predictions.

478   Over the whole period at Melpitz, the median N_{CCN} and AR increased from 399 to

479   2144 cm^{-3} and 0.10 to 0.48 with SS increasing from 0.1% to 0.7%, respectively. Aerosol

480   activation characteristics are highly variable across seasons, especially at relatively low

481   SS conditions. For instance at $SS = 0.1\%$, the median N_{CCN} and AR in winter are 1.6 and

482   2.3 times higher than the summer values, respectively. Aerosol particle activation

483   depends on its physical and chemical properties. In summer, the highest N_{aero}, smallest

484   *GMD,* and lowest κ_{chem} all contribute to the lowest AR and N_{CCN} among the four seasons,

485   and the reverse holds true in winter. Additionally, in summer, the steepest PNSD in 40-

486   200 nm size range and the lowest κ_{chem} causes the strongest sensitivity of N_{CCN} and AR

487   to *SS* even though the spread in κ_{CCN} is narrowest.

488   Both κ and the mixing state are size-dependent, thereby varying with *SS*. The

489   median κ_{CCN} decreases from 0.27 to 0.19 as *SS* increases from 0.1% to 0.7%, which

490   was less than the median bulk κ_{chem}. The seasonal trend of κ_{CCN} was similar to that of

491   κ_{chem}, especially at relatively low *SS* conditions. The lowest κ_{CCN} and κ_{chem} were

492   observed in summer, which related to the highest organics mass fraction in particles.

493   Aerosol particles were more internally mixed in summer and spring whereas less

494   internally mixed in winter and autumn. In cold seasons, the increasing anthropogenic

495   emissions linked to house heating mixed with the aged particles from long-range

496   transport, which could decrease the degree of external mixing of particles. As D_p

497   increases, κ_{CCN} increases at D_p range of ~40 to 100 nm and almost stays constant at D_p

498   range of 100 to 200 nm, whereas the $(D_{75} - D_{25})/D_c$ monotonically decreases. The

499   relationships of $(D_{75} - D_{25})/D_c$ vs. D_p and κ vs. D_p are both fitted well by a power-law

500   function for each season.

501   Five activation schemes are evaluated on the N_{CCN} predictions. Compared to using

502   the classic N_{CCN} - *SS* or AR - *SS* power-law fits to predict N_{CCN}, the prediction is better

503   by using the real-time PNSD combined with the parameterized κ, including a constant

504   κ of 0.3, the bulk κ_{chem}, and the κ - D_p power-law fit. However, assuming a constant κ

505   of 0.3 recommended for continental aerosol (Andreae and Rosenfeld., 2008) or the bulk

506   κ_{chem} calculated from aerosol chemical composition both cause significant

507   overestimations of the N_{CCN} with approximately 10% in median for all *SS* conditions,

508 which theoretically cause 3.2% overestimation of cloud optical thickness, amounting to

509 approximately one-third of the direct radiative forcing from a doubling CO_2 (Lee et al.,

510 1997). And, the strength of the autoconversion process in cloud could be

511 underestimated (Liu et al., 2006). Size-resolved κ improves the N_{CCN} prediction. We

512 recommend applying the κ - D_p power-law fit for N_{CCN} prediction, which obtains the

513 best prediction among the five schemes.

514   The κ - D_p power-law fit presented in this study could apply to other rural regions.

515 However, it may cause considerable deviations for different aerosol background regions.

516 For instance, using the κ - D_p power-law fit measured in urban Budapest (Salma et al.,

517 2021) for predicting Melpitz N_{CCN}, it could cause a 39% underestimation of N_{CCN} in

518 median for all SS conditions. Additionally, the seasonal difference of the κ - D_p

519 relationship needs to be considered carefully for N_{CCN} prediction. At Melpitz, if the κ -

520 D_p power-law fit measured in summer was used for predicting N_{CCN} in winter, it could

521 cause a 13% underestimation of N_{CCN} in median for all SS conditions. Although the κ -

522 D_p relationships are similar measured in rural stations, but when comparing the different

523 urban stations (e.g., shanghai vs. Budapest in Figure 8), these relationships are clearly

524 different and the reasons for the difference are still unclear. Thus, long-term

525 monodisperse CCN measurements are still needed not only to obtain the κ - D_p

526 relationships for different regions and for different seasons, but furtherly investigate the

527 reasons for the difference of the κ - D_p relationships measured at same type of regions.

528 Finally for the purpose of predicting N_{CCN}, the measurements of monodisperse CCN

529 and particle chemical compositions are more expected, compared to the polydisperse

530 CCN measurements.

531

532 **Appendix Notation list**

A	comprehensive parameter for $\sigma_{s/a}$, M_w, R, T, and ρ_w in equation (2b)
a	lower limit for calculating critical diameters at the set-nominal supersaturations in equation (1)
ACI	aerosol and cloud interactions
ACSM	aerosol chemical species monitor
ACTRIS	Aerosol, Clouds and Trace Gases Research Infrastructure
AF	activated fraction, i.e., N_{CCN}/N_{CN}
AIEs	aerosol indirect effects
AR	activation ratio, i.e., N_{CCN}/N_{aero}
b	upper limit for calculating critical diameters at the set-nominal supersaturations in equation (1)
BC	black carbon
CN	condensation nuclei
CCN	cloud condensation nuclei
CCNC	cloud condensation nuclei counter
$coef$	coefficient in κ - D_p power-law fit
CPC	condensation particle counter
D_p	diameter of the dry particle
D_c	critical diameter of the dry particle
D_X	D at which X % of the particles are activated
$(D_{75} - D_{25})/D_c$	degree of external mixture
D-MPSS	Dual-mobility particle size spectrometer
DMA	differential mobility analyzer
eBC	equivalent black carbon
f_{BC}	mass fraction of BC in submicron aerosol
$f_{nitrate}$	mass fraction of nitrate in submicron aerosol
f_{org}	mass fraction of organics in submicron aerosol
$f_{sulfate}$	mass fraction of sulfate in submicron aerosol
GMD	geometric mean diameter of PNSD
M_w	molecular weight of water
N_{aero}	number concentration of aerosol with a D_p range of 10 to 800 nm
N_C	number concentration of cloud droplet
N_{CN}	number concentration of CN
N_{CCN}	number concentration of CCN
NPF	new particle formation
OA	organic aerosol
PM_{10}	particulate matter with the $D_p < 10$ μm
PNSD	particle number size distribution
R	universal gas constant
R^2	coefficient of determination
RD	relative deviation between the predicted N_{CCN} and the measured one
SI	Supporting information

SS	supersaturation
SOA	secondary organic aerosol
T	temperature
σ_s	represent the shape of the sigmoid function
$\sigma_{s/a}$	droplet surface tension
κ	hygroscopicity factor of aerosol particle
κ_i	κ *of* each component
κ_{CCN}	κ calculated from the monodisperse CCN measurements
κ_{chem}	κ calculated from the aerosol chemical measurements
ε_i	volume fraction of each component
ρ_w	density of the liquid water

533

534 ***Data availability.***

535 The data used in this study are available from Silvia Henning (henning@tropos.de)

536 upon request and https://doi.org/10.1594/PANGAEA.938215.

537 ***Author contributions.***

538 AW, SH and LP designed the research. SH and LP collected the data at Melpitz. YW

539 performed the data analysis and prepared the paper. All co-authors contributed to

540 interpretation of the results as well as paper review and editing.

541 ***Competing interests.***

542 The authors declare that they have no conflict of interest.

543 ***Acknowledgments.***

544 This research has been supported by the H2020 research infrastructures (grant nos.

545 ACTRIS (262254) and ACTRIS-2 (654109)), the European Cooperation in Science and

546 Technology (grant no. COLOSSAL CA16109), the German Federal Environment

547 Ministry (BMU) grants F&E 370343200 (German title: "Erfassung der Zahl feiner und

548 ultrafeiner Partikel in der Außenluft"), 2008–2010, and F&E 371143232 (German title:

549 "Trendanalysen gesundheitsgefährdender Fein- und Ultrafeinstaubfraktionen unter

550 Nutzung der im German Ultrafine Aerosol Network (GUAN) ermittelten

Immissionsdaten durch Fortführung und Interpretation der Messreihen"), 2012–2014. This research has received funding from the Deutsche Forschungsgemeinschaft (*DFG*, German Research Foundation, HE 6770/2), the National Natural Science Foundation of China under grant numbers 42205072, 42075066, 42075063, 42175099, and 42005067. The China Scholarship Council (no.202008320513) is acknowledged for supporting Yuan Wang financially. We thank Achim Grüner and René Rabe for the careful maintenance of the measurements on site. We also thank Angela Buchholz and another anonymous reviewer for their helpful comments and suggestions on improving the paper.

References

Albrecht, B. A.: Aerosols, cloud microphysics, and fractional cloudiness, Science, 245(4923), 1227–1230, https://doi.org/10.1126/ science.245.4923.1227, 1989.

Andreae, M. O. and Rosenfeld, D.: Aerosol-cloud-precipitation interactions. Part 1. The nature and sources of cloud-active particles, Earth-Sci. Rev., 89, 13–41, https://doi.org/10.1016/j.earscirev.2008.03.001, 2008.

Birmili, W., Stratmann, F., and Wiedensohler, A.: Design of a DMA-based size spectrometer for a large particle size range and stable operation, J. Aerosol Sci., 30, 549–553, https://doi.org/10.1016/S0021-8502(98)00047-0, 1999.

Birmili, W., Weinhold, K., Nordmann, S., Wiedensohler, A., Spindler, G., Müller, K., Herrmann, H., Gnauk, T., Pitz, M., Cyrys, J., Flentje, H., Nickel, C., Kuhlbusch, T. A. J., and Löschau, G.: Atmospheric aerosol measurements in the German Ultrafine Aerosol Network (GUAN): Part 1 – soot and particle number size distribution, Gefahrst. Reinh. Luft., 69, 137–145, 2009.

Burkart, J., Steiner, G., Reischl, G., and Hitzenberger, R.: Longterm study of cloud condensation nuclei (CCN) activation of the atmospheric aerosol in Vienna, Atmos. Environ., 45, 5751–5759, https://doi.org/10.1016/j.atmosenv.2011.07.022, 2011.

Che, H., Zhang, X., Zhang, L., Wang, Y., Shen, X., Ma, Q., Sun, J., Zhong, J.: Prediction of size-resolved number concentration of cloud condensation nuclei and long-term measurements of their activation characteristics, Sci. Rep., 7, 5819, https://doi.org/10.1038/s41598-017-05998-3, 2017.

Chen, G., Canonaco, F., Tobler, A., Aas, W., Alastuey, A., Allan, J., Atabakhsh, S., Aurela, M., Baltensperger, U., Bougiatioti, A., Brito, J. F. D., Ceburnis, D., Chazeau, B., Chebaicheb, H., Daellenbach, K. R., Ehn, M., Haddad, I. E., Eleftheriadis, K., Favez, O., Flentje, H., Font, A., Fossum, K., Freney, E., Gini, M., Green, D. C., Heikkinen, L., Herrmann, H., Kalogridis, A., Keernik, H., Lhotka, R., Lin, C., Lunder, C., Maasikmets, M., Manousakas, M. I., Marchand, N., Marin, C., Marmureanu, L., Mihalopoulos, N., Močnik, G., Nęcki, J., O'Dowd, C., Ovadnevaite, J., Peter, T., Petit, J., Pikridas, M., Platt, S.M., Pokorná, P., Poulain, L., Priestman, M., Riffault, V., Rinaldi, M., Różański, K., Schwarz, J., Sciare, J., Simon, L., Skiba, A., Slowik, J. G., Sosedova, Y., Stavroulas, I., Styszko, K., Teinemaa, E., Timonen, H., Tremper, A., Vasilescu, J., Via, M., Vodička, P., Wiedensohler, A., Zografou, O., Minguillón, M.C., Prévôt, A.S.H.: European aerosol phenomenology − 8: Harmonised source apportionment of organic aerosol using 22 Year-long ACSM/AMS datasets, Environ. Int., 166, 107325, 2002.

Chen, L., Zhang, F., Zhang, D., Wang, X., Song, W., Liu, J., Ren, J., Jiang, S., Li, X., and Li, Z.: Measurement report: Hygroscopic growth of ambient fine particles measured at five sites in China, Atmos. Chem. Phys., 22, 6773–6786, https://doi.org/10.5194/acp-22-6773-2022, 2022.

Clegg, S., Brimblecombe, P., and Wexler, A.: Thermodynamic model of the system H^+ - NH_4^+ - SO_4^{2-} - NO_3^- - H_2O at tropospheric temperatures. J. Phys. Chem. A, 102, 2137-2154,1998.

Crenn, V., Sciare, J., Croteau, P. L., Verlhac, S., Fröhlich, R., Belis, C. A., Aas, W., Äijälä, M.,

Alastuey, A., Artiñano, B., Baisnée, D., Bonnaire, N., Bressi, M., Canagaratna, M., Canonaco, F., Carbone, C., Cavalli, F., Coz, E., Cubison, M. J., Esser-Gietl, J. K., Green, D. C., Gros, V., Heikkinen, L., Herrmann, H., Lunder, C., Minguillón, M. C., Močnik, G., O'Dowd, C. D., Ovadnevaite, J., Petit, J.-E., Petralia, E., Poulain, L., Priestman, M., Riffault, V., Ripoll, A., Sarda-Estève, R., Slowik, J. G., Setyan, A., Wiedensohler, A., Baltensperger, U., Prévôt, A. S. H., Jayne, J. T., and Favez, O.: ACTRIS ACSM intercomparison – Part 1: Reproducibility of concentration and fragment results from 13 individual Quadrupole Aerosol Chemical Speciation Monitors (Q-ACSM) and consistency with co-located instruments, Atmos. Meas. Tech., 8, 5063–5087, https://doi.org/10.5194/amt-8-5063-2015, 2015.

Crippa, M., Canonaco, F., Lanz, V. A., Äijälä, M., Allan, J. D., Carbone, S., Capes, G., Ceburnis, D., Dall'Osto, M., Day, D. A., DeCarlo, P. F., Ehn, M., Eriksson, A., Freney, E., Hildebrandt Ruiz, L., Hillamo, R., Jimenez, J. L., Junninen, H., Kiendler-Scharr, A., Kortelainen, A.-M., Kulmala, M., Laaksonen, A., Mensah, A. A., Mohr, C., Nemitz, E., O'Dowd, C., Ovadnevaite, J., Pandis, S. N., Petäjä, T., Poulain, L., Saarikoski, S., Sellegri, K., Swietlicki, E., Tiitta, P., Worsnop, D. R., Baltensperger, U., and Prévôt, A. S. H.: Organic aerosol components derived from 25 AMS data sets across Europe using a consistent ME-2 based source apportionment approach, Atmos. Chem. Phys., 14, 6159–6176, https://doi.org/10.5194/acp-14-6159-2014, 2014.

Croft, B., Lohmann, U., Martin, R. V., Stier, P., Wurzler, S., Feichter, J., Posselt, R., and Ferrachat, S.: Aerosol size-dependent below-cloud scavenging by rain and snow in the ECHAM5-HAM, Atmos. Chem. Phys., 9, 4653–4675, https://doi.org/10.5194/acp-9-4653-2009, 2009.

Deng, Z. Z., Zhao, C. S., Ma, N., Liu, P. F., Ran, L., Xu, W. Y., Chen, J., Liang, Z., Liang, S., Huang, M. Y., Ma, X. C., Zhang, Q., Quan, J. N., Yan, P., Henning, S., Mildenberger, K., Sommerhage, E., Schäfer, M., Stratmann, F., and Wiedensohler, A.: Size-resolved and bulk activation properties of aerosols in the North China Plain, Atmos. Chem. Phys., 11, 3835–3846, https://doi.org/10.5194/acp-11-3835-2011, 2011.

Deng, Z. Z., Zhao, C. S., Ma, N., Ran, L., Zhou, G. Q., Lu, D. R., and Zhou, X. J.: An examination of parameterizations for the CCN number concentration based on in situ measurements of aerosol activation properties in the North China Plain, Atmos. Chem. Phys., 13, 6227–6237, https://doi.org/10.5194/acp-13-6227-2013, 2013.

Dusek, U., Frank, G., Hildebrandt, L., Curtius, J., Schneider, J., Walter, S., Chand, D., Drewnick, F., Hings, S., Jung, D., Borrmann, S., and Andreae, M. O.: Size matters more than chemistry for cloud-nucleating ability of aerosol particles. Science, 312(5778): 1375-1378, DOI: 10.1126/science.1125261, 2006.

Dusek, U., Frank, G., Curtius, J., Drewnick, F., Schneider, J., Kürten, A., Rose, D., Andreae, M. O., Borrmann, S., Pöschl, U.: Enhanced organic mass fraction and decreased hygroscopicity of cloud condensation nuclei (CCN) during new particle formation events, Geophys. Res. Lett. 37 (3), doi: 10.1029/2009GL040930, 2010.

Eichler, H., Cheng, Y. F., Birmili, W., Nowak, A., Wiedensohler, A., Brüggemann, E., Gnauk, T.,

Herrmann, H., Althausen, D., Ansmann, A., Engelmann, R., Tesche, M., Wendisch, M., Zhang, Y. H., Hu, M., Liu, S., and Zeng, L. M.: Hygroscopic properties and extinction of aerosol particles at ambient relative humidity in South-Eastern China, Atmos. Environ., 42, 6321–6334, https://doi.org/10.1016/j.atmosenv.2008.05.007, 2008.

Fan, J., Leung, L. R., Li, Z., Morrison, H., Chen, H., Zhou, Y., Qian, Y., and Wang, Y.: Aerosol impacts on clouds and precipitation in eastern China: Results from bin and bulk microphysics, J. Geophys. Res., 117, D00K36, https://doi.org/10.1029/2011JD016537, 2012.

Fan, J., Rosenfeld, D., Zhang, Y., Giangrande, S. E., Li, Z., Machado, L. A. T., Martin, S. T., Yang, Y., Wang, J., Artaxo, P., Barbosa, H. M. J., Braga, R. C., Comstock, J. M., Feng, Z., Gao, W., Gomes, H. B., Mei, F., Pöhlker, C., Pöhlker, M. L., Pöschl, U., and Souza, R. A. F.: Substantial convection and precipitation enhancements by ultrafine aerosol particles, Science, 359(6374), 411–418, DOI: 10.1126/science.aan8461, 2018.

Fors, E. O., Swietlicki, E., Svenningsson, B., Kristensson, A., Frank, G. P., and Sporre, M.: Hygroscopic properties of the ambient aerosol in southern Sweden – a two year study, Atmos. Chem. Phys., 11, 8343–8361, https://doi.org/10.5194/acp-11-8343-2011, 2011.

Freney, E., Zhang, Y., Croteau, P., Amodeo, T., Williams, L., Truong, F., Petit, J.-E., Sciare, J., Sarda-Esteve, R., Bonnaire, N., Arumae, T., Aurela, M., Bougiatioti, A., Mihalopoulos, N., Coz, E., Artinano, B., Crenn, V., Elste, T., Heikkinen, L., Poulain, L., Wiedensohler, A., Herrmann, H., Priestman, M., Alastuey, A., Stavroulas, I., Tobler, A., Vasilescu, J., Zanca, N., Canagaratna, M., Carbone, C., Flentje, H., Green, D., Maasikmets, M., Marmureanu, L., Minguillon, M. C., Prevot, A. S. H., Gros, V., Jayne, J., and Favez, O.: The second ACTRIS inter-comparison (2016) for Aerosol Chemical Speciation Monitors (ACSM): Calibration protocols and instrument performance evaluations, Aerosol Sci. Tech., 53, 830–842, https://doi.org/10.1080/02786826.2019.1608901, 2019.

Gunthe, S. S., King, S. M., Rose, D., Chen, Q., Roldin, P., Farmer, D. K., Jimenez, J. L., Artaxo, P., Andreae, M. O., Martin, S. T., and Pöschl, U.: Cloud condensation nuclei in pristine tropical rainforest air of Amazonia: size–esolved measurements and modeling of atmospheric aerosol composition and CCN activity, Atmos. Chem. Phys., 9, 7551–7575, https://doi.org/10.5194/acp-9-7551-2009, 2009.

Gunthe, S. S., Rose, D., Su, H., Garland, R. M., Achtert, P., Nowak, A., Wiedensohler, A., Kuwata, M., Takegawa, N., Kondo, Y., Hu, M., Shao, M., Zhu, T., Andreae, M. O., and Pöschl, U.: Cloud condensation nuclei (CCN) from fresh and aged air pollution in the megacity region of Beijing, Atmos. Chem. Phys., 11, 11023–11039, https://doi.org/10.5194/acp-11-11023-2011, 2011.

Gysel, M., Crosier, J., Topping, D. O., Whitehead, J. D., Bower, K. N., Cubison, M. J., Williams, P. I., Flynn, M. J., McFiggans, G. B., and Coe, H.: Closure study between chemical composition and hygroscopic growth of aerosol particles during TORCH2, Atmos. Chem. Phys., 7, 6131–6144, doi:10.5194/acp-7-6131-2007, 2007.

Gysel, M. and Stratmann, F.: WP3 – NA3: In-situ chemical, physical and optical properties of aerosols, Deliverable D3.11: Standardized protocol for CCN measurements, Tech. rep., http:// https://actris-ecac.eu/ccn-nc.html, 2013.

Henning, S., Dieckmann, K., Ignatius, K., Schäfer, M., Zedler, P., Harris, E., Sinha, B., van Pinxteren, D., Mertes, S., Birmili, W., Merkel, M., Wu, Z., Wiedensohler, A., Wex, H., Herrmann, H., and Stratmann, F.: Influence of cloud processing on CCN activation behaviour in the Thuringian Forest, Germany during HCCT-2010, Atmos. Chem. Phys., 14, 7859–7868, https://doi.org/10.5194/acp-14-7859-2014, 2014.

IPCC.: Climate Change 2021: The Physical Science Basis. Contribution of Working Group I to the Sixth Assessment Report of the Intergovernmental Panel on Climate Change, (p. 1796), Cambridge University Press. In Press, 2021.

Jayachandran, V. N., Varghese, M., Murugavel, P., Todekar, K. S., Bankar, S. P., Malap, N., Dinesh, G., Safai, P. D., Rao, J., Konwar, M., Dixit, S., and Prabha, T. V.: Cloud condensation nuclei characteristics during the Indian summer monsoon over a rain-shadow region, Atmos. Chem. Phys., 20, 7307–7334, https://doi.org/10.5194/acp-20-7307-2020, 2020.

Jia, H., Ma, X., Yu, F., Liu, Y., Yin, Y.: Distinct impacts of increased aerosols on cloud droplet number concentration of stratus/stratocumulus and cumulus. Geophys. Res. Lett., 46(22): 13517–13525, https://doi.org/10.1029/2019GL085081, 2019.

Jurányi, Z., Tritscher, T., Gysel, M., Laborde, M., Gomes, L., Roberts, G., Baltensperger, U., and Weingartner, E.: Hygroscopic mixing state of urban aerosol derived from size-resolved cloud condensation nuclei measurements during the MEGAPOLI campaign in Paris, Atmos. Chem. Phys., 13, 6431–6446, https://doi.org/10.5194/acp-13-6431-2013, 2013.

Khain, P. A.: Notes on state-of-the-art investigations of aerosol effects on precipitation: A critical review, Environ. Res. Lett., 4(1), 015004, DOI: 10.1088/1748-9326/4/1/015004, 2009.

Kim, J. H., Yum, S. S., Shim, S., Kim, W. J., Park, M., Kim, J.-H., Kim, M.-H., and Yoon, S.-C.: On the submicron aerosol distributions and CCN number concentrations in and around the Korean Peninsula, Atmos. Chem. Phys., 14, 8763–8779, https://doi.org/10.5194/acp-14-8763-2014, 2014.

Köhler, H.: The nucleus in and the growth of hygroscopic droplets, Trans Farad Soc, 32, 1152–1161, https://doi.org/10.1039/TF9363201152, 1936.

Kristensen, T. B., Müller, T., Kandler, K., Benker, N., Hartmann, M., Prospero, J. M., Wiedensohler, A., and Stratmann, F.: Properties of cloud condensation nuclei (CCN) in the trade wind marine boundary layer of the western North Atlantic, Atmos. Chem. Phys., 16, 2675–2688, https://doi.org/10.5194/acp-16-2675-2016, 2016.

Kuang, Y., He, Y., Xu, W., Zhao, P., Cheng, Y., Zhao, G., Tao, J., Ma, N., Su, H., Zhang, Y., Sun, J., Cheng, P., Yang, W., Zhang, S., Wu, C., Sun, Y., and Zhao, C.: Distinct diurnal variation in organic aerosol hygroscopicity and its relationship with oxygenated organic aerosol, Atmos. Chem. Phys., 20, 865–880, https://doi.org/10.5194/acp-20-865-2020, 2020.

Kulmala, M., Petäjä, T., Nieminen, T., Sipilä, M., Manninen, H. E., Lehtipalo, K., Dal Maso, M., Aalto, P. P., Junninen, H., Paasonen, P., Riipinen, I., Lehtinen, K. E. J., Laaksonen, A., and Kerminen, V.-M.: Measurement of the nucleation of atmospheric aerosol particles, Nat. Protocols, 7, 1651–1667, https://doi.org/10.1038/nprot.2012.091, 2012.

Lee, W., Iacobellis, S. F., and Somerville, R. C. J.: Cloud Radiation Forcings and Feedbacks: General Circulation Model Tests and Observational Validation, Journal of Climate, 10(10), 2479-2496, 1997.

Liu, Y., Daum, P. H., McGraw, R., and Miller, M.: Generalized threshold function accounting for effect of relative dispersion on threshold behavior of autoconversion process, Geophys. Res. Lett., 33(11), L11804, 2006.

Liu, J. and Li, Z.: Estimation of cloud condensation nuclei concentration from aerosol optical quantities: influential factors and uncertainties, Atmos. Chem. Phys., 14, 471–483, https://doi.org/10.5194/acp-14-471-2014, 2014.

Ma, N. and Birmili, W.: Estimating the contribution of photochemical particle formation to ultrafine particle number averages in an urban atmosphere, Sci. Total Environ., 512/513, 154–166, https://doi.org/10.1016/j.scitotenv.2015.01.009, 2015

Massling, A., Stock, M., Wehner, B., Wu, Z. J., Hu, M., Brueggemann, E., Gnauk, T., Herrmann, H., and Wiedensohler, A.: Size segregated water uptake of the urban submicrometer aerosol in Beijing, Atmos. Environ., 43, 1578–1589, https://doi.org/10.1016/j.atmosenv.2008.06.003, 2009.

Mazoyer, M., Burnet, F., Denjean, C., Roberts, G. C., Haeffelin, M., Dupont, J.-C., and Elias, T.: Experimental study of the aerosol impact on fog microphysics, Atmos. Chem. Phys., 19, 4323–4344, https://doi.org/10.5194/acp-19-4323-2019, 2019.

Müller, T., Henzing, J. S., de Leeuw, G., Wiedensohler, A., Alastuey, A., Angelov, H., Bizjak, M., Collaud Coen, M., Engström, J. E., Gruening, C., Hillamo, R., Hoffer, A., Imre, K., Ivanow, P., Jennings, G., Sun, J. Y., Kalivitis, N., Karlsson, H., Komppula, M., Laj, P., Li, S.-M., Lunder, C., Marinoni, A., Martins dos Santos, S., Moerman, M., Nowak, A., Ogren, J. A., Petzold, A., Pichon, J. M., Rodriquez, S., Sharma, S., Sheridan, P. J., Teinilä, K., Tuch, T., Viana, M., Virkkula, A., Weingartner, E., Wilhelm, R., and Wang, Y. Q.: Characterization and intercomparison of aerosol absorption photometers: result of two intercomparison workshops, Atmos. Meas. Tech., 4, 245–268, https://doi.org/10.5194/amt-4-245-2011, 2011

Nenes, A., Charlson, R. J., Facchini, M. C., Kulmalam M., Laaksonen, A., and Seinfeld, J. H.: Can chemical effects on cloud droplet number rival the first indirect effect? Geophys. Res. Lett., 29(17): 29-1-29-4, doi:10.1029/2002GL015295, 2002.

Ng, N. L., Herndon, S. C., Trimborn, A., Canagaratna, M. R., Croteau, P. L., Onasch, T. B., Sueper, D., Worsnop, D. R., Zhang, Q., Sun, Y. L., and Jayne, J. T.: An Aerosol Chemical Speciation Monitor (ACSM) for Routine Monitoring of the Composition and Mass Concentrations of Ambient Aerosol, Aerosol Sci. Tech., 45, 780–794,

https://doi.org/10.1080/02786826.2011.560211, 2011.

Ovadnevaite, J., Zuend, A., Laaksonen, A., Sanchez, K. J., Roberts, G., Ceburnis, D., Decesari, S., Rinaldi, M., Hodas, N., Facchini, M. C., Seinfeld, J. H. and O' Dowd, C.: Surface tension prevails over solute effect in organic-influenced cloud droplet activation, Nature, 546(7660), 637–641, doi:10.1038/nature22806, 2017.

Paramonov, M., Kerminen, V.-M., Gysel, M., Aalto, P. P., Andreae, M. O., Asmi, E., Baltensperger, U., Bougiatioti, A., Brus, D., Frank, G. P., Good, N., Gunthe, S. S., Hao, L., Irwin, M., Jaatinen, A., Jurányi, Z., King, S. M., Kortelainen, A., Kristensson, A., Lihavainen, H., Kulmala, M., Lohmann, U., Martin, S. T., McFiggans, G., Mihalopoulos, N., Nenes, A., O'Dowd, C. D., Ovadnevaite, J., Petäjä, T., Pöschl, U., Roberts, G. C., Rose, D., Svenningsson, B., Swietlicki, E., Weingartner, E., Whitehead, J., Wiedensohler, A., Wittbom, C., and Sierau, B.: A synthesis of cloud condensation nuclei counter (CCNC) measurements within the EUCAARI network, Atmos. Chem. Phys., 15, 12211–12229, https://doi.org/10.5194/acp-15-12211-2015, 2015.

Petters, M. D., and Kreidenweis, S. M.: A single parameter representation of hygroscopic growth and cloud condensation nuclei activity, Atmos. Chem. Phys., 7, 1961-1971, https://doi.org/10.5194/acp-7-1961-2007, 2007.

Petzold, A. and Schönlinner, M.: Multi-angle absorption photometry - a new method for the measurement of aerosol light absorption and atmospheric black carbon, J. Aerosol Sci., 35, 421–441, https://doi.org/10.1016/j.jaerosci.2003.09.005, 2004.

Poulain, L., Wu, Z., Petters, M. D., Wex, H., Hallbauer, E., Wehner, B., Massling, A., Kreidenweis, S. M., and Stratmann, F.: Towards closing the gap between hygroscopic growth and CCN activation for secondary organic aerosols – Part 3: Influence of the chemical composition on the hygroscopic properties and volatile fractions of aerosols, Atmos. Chem. Phys., 10, 3775–3785, https://doi.org/10.5194/acp-10-3775-2010, 2010.

Poulain, L., Spindler, G., Birmili, W., Plass-Dülmer, C., Wiedensohler, A., and Herrmann, H.: Seasonal and diurnal variations of particulate nitrate and organic matter at the IfT research station Melpitz, Atmos. Chem. Phys., 11, 12579–12599, https://doi.org/10.5194/acp-11-12579-2011, 2011.

Poulain, L., Birmili, W., Canonaco, F., Crippa, M., Wu, Z. J., Nordmann, S., Spindler, G., Prévôt, A. S. H., Wiedensohler, A., and Herrmann, H.: Chemical mass balance of 300 °C non-volatile particles at the tropospheric research site Melpitz, Germany, Atmos. Chem. Phys., 14, 10145–10162, https://doi.org/10.5194/acp-14-10145-2014, 2014.

Poulain, L., Spindler, G., Grüner, A., Tuch, T., Stieger, B., van Pinxteren, D., Petit, J.-E., Favez, O., Herrmann, H., and Wiedensohler, A.: Multi-year ACSM measurements at the central European research station Melpitz (Germany) – Part 1: Instrument robustness, quality assurance, and impact of upper size cutoff diameter, Atmos. Meas. Tech., 13, 4973–4994, https://doi.org/10.5194/amt-13-4973-2020, 2020.

Pöhlker, M. L., Pöhlker, C., Ditas, F., Klimach, T., Hrabe de Angelis, I., Araújo, A., Brito, J.,

Carbone, S., Cheng, Y., Chi, X., Ditz, R., Gunthe, S. S., Kesselmeier, J., Könemann, T., Lavrič, J. V., Martin, S. T., Mikhailov, E., Moran-Zuloaga, D., Rose, D., Saturno, J., Su, H., Thalman, R., Walter, D., Wang, J., Wolff, S., Barbosa, H. M. J., Artaxo, P., Andreae, M. O., and Pöschl, U.: Long-term observations of cloud condensation nuclei in the Amazon rain forest – Part 1: Aerosol size distribution, hygroscopicity, and new model parametrizations for CCN prediction, Atmos. Chem. Phys., 16, 15709–15740, https://doi.org/10.5194/acp-16-15709-2016, 2016.

Pöhlker, M. L., Ditas, F., Saturno, J., Klimach, T., Hrabě de Angelis, I., Araùjo, A. C., Brito, J., Carbone, S., Cheng, Y., Chi, X., Ditz, R., Gunthe, S. S., Holanda, B. A., Kandler, K., Kesselmeier, J., Könemann, T., Krüger, O. O., Lavrič, J. V., Martin, S. T., Mikhailov, E., Moran-Zuloaga, D., Rizzo, L. V., Rose, D., Su, H., Thalman, R., Walter, D., Wang, J., Wolff, S., Barbosa, H. M. J., Artaxo, P., Andreae, M. O., Pöschl, U., and Pöhlker, C.: Long-term observations of cloud condensation nuclei over the Amazon rain forest – Part 2: Variability and characteristics of biomass burning, long-range transport, and pristine rain forest aerosols, Atmos. Chem. Phys., 18, 10289–10331, https://doi.org/10.5194/acp-18-10289-2018, 2018.

Ramanathan, V., Crutzen, P. J., Kiehl, J. T., and Rosenfeld, D.: Aerosols, climate, and the hydrological cycle, Science, 294(5549), 2119–2124. https://doi.org/10.1126/science.1064034, 2001.

Rastak, N., Pajunoja, A., Acosta Navarro, J. C., Ma, J., Song, M., Partridge, D. G., Kirkevåg, A., Leong, Y., Hu, W. W., Taylor, N. F., Lambe, A., Cerully, K., Bougiatioti, A., Liu, P., Krejci, R., Petäjä, T., Percival, C., Davidovits, P., Worsnop, D. R., Ekman, A. M. L., Nenes, A., Martin, S., Jimenez, J. L., Collins, D. R., Topping, D. O., Bertram, A. K., Zuend, A., Virtanen, A., and Riipinen, I.: Microphysical explanation of the RH-dependent water affinity of biogenic organic aerosol and its importance for climate, Geophys. Res. Lett., 44, 5167–5177, https://doi.org/10.1002/2017gl073056, 2017.

Roberts, G. C., and Nenes, A.: A continuous-flow streamwise thermal-gradient CCN chamber for atmospheric measurements, Aerosol Sci. Tech., 39(3), 206–221, https://doi.org/10.1080/027868290913988, 2005.

Rose, D., Gunthe, S. S., Mikhailov, E., Frank, G. P., Dusek, U., Andreae, M. O., and Pöschl, U.: Calibration and measurement uncertainties of a continuous-flow cloud condensation nuclei counter (DMT-CCNC): CCN activation of ammonium sulfate and sodium chloride aerosol particles in theory and experiment, Atmos. Chem. Phys., 8, 1153–1179, https://doi.org/10.5194/acp-8-1153-2008, 2008.

Rose, D., Nowak, A., Achtert, P., Wiedensohler, A., Hu, M., Shao, M., Zhang, Y., Andreae, M. O., and Pöschl, U.: Cloud condensation nuclei in polluted air and biomass burning smoke near the mega-city Guangzhou, China – Part 1: Size-resolved measurements and implications for the modeling of aerosol particle hygroscopicity and CCN activity, Atmos. Chem. Phys., 10, 3365–3383, https://doi.org/10.5194/acp-10-3365-2010, 2010.

Rose, D., Gunthe, S. S., Su, H., Garland, R. M., Yang, H., Berghof, M., Cheng, Y. F., Wehner, B.,

827   Achtert, P., Nowak, A., Wiedensohler, A., Takegawa, N., Kondo, Y., Hu, M., Zhang, Y.,
828   Andreae, M. O., and Pöschl, U.: Cloud condensation nuclei in polluted air and biomass burning
829   smoke near the megacity Guangzhou, China – Part 2: Size-resolved aerosol chemical
830   composition, diurnal cycles, and externally mixed weakly CCN-active soot particles, Atmos.
831   Chem. Phys., 11, 2817–2836, https://doi.org/10.5194/acp-11-2817-2011, 2011

832   Rosenfeld, D., Zhu, Y., Wang, M., Zheng, Y., Goren, T., and Yu, S.: Aerosol-driven droplet
833   concentrations dominate coverage and water of oceanic low-level clouds, science, 363(6427),
834   DOI: 10.1126/science.aav0566, 2019.

835   Salma, I., Thén, W., Vörösmarty, M., and Gyöngyösi, A. Z.: Cloud activation properties of aerosol
836   particles in a continental Central European urban environment, Atmos. Chem. Phys., 21,
837   11289–11302, https://doi.org/10.5194/acp-21-11289-2021, 2021.

838   Schmale, J., Henning, S., Decesari, S., Henzing, B., Keskinen, H., Sellegri, K., Ovadnevaite, J.,
839   Pöhlker, M. L., Brito, J., Bougiatioti, A., Kristensson, A., Kalivitis, N., Stavroulas, I., Carbone,
840   S., Jefferson, A., Park, M., Schlag, P., Iwamoto, Y., Aalto, P., Äijälä, M., Bukowiecki, N., Ehn,
841   M., Frank, G., Fröhlich, R., Frumau, A., Herrmann, E., Herrmann, H., Holzinger, R., Kos, G.,
842   Kulmala, M., Mihalopoulos, N., Nenes, A., O'Dowd, C., Petäjä, T., Picard, D., Pöhlker, C.,
843   Pöschl, U., Poulain, L., Prévôt, A. S. H., Swietlicki, E., Andreae, M. O., Artaxo, P.,
844   Wiedensohler, A., Ogren, J., Matsuki, A., Yum, S. S., Stratmann, F., Baltensperger, U., and
845   Gysel, M.: Long-term cloud condensation nuclei number concentration, particle number size
846   distribution and chemical composition measurements at regionally representative observatories,
847   Atmos. Chem. Phys., 18, 2853–2881, https://doi.org/10.5194/acp-18-2853-2018, 2018.

848   Seinfeld, J. H., and Pandis, S. N.: Atmospheric chemistry and physics: From air pollution to climate
849   change, Hoboken: John Wiley and Sons, 2016.

850   Sihto, S.-L., Mikkilä, J., Vanhanen, J., Ehn, M., Liao, L., Lehtipalo, K., Aalto, P. P., Duplissy, J.,
851   Petäjä, T., Kerminen, V.-M., Boy, M., and Kulmala, M.: Seasonal variation of CCN
852   concentrations and aerosol activation properties in boreal forest, Atmos. Chem. Phys., 11,
853   13269–13285, https://doi.org/10.5194/acp-11-13269-2011, 2011.

854   Singla, V., Mukherjee, S., Safai, P. D., Meena, G. S., Dani, K. K., Pandithurai, G.: Role of organic
855   aerosols in CCN activation and closure over a rural background site in Western Ghats, India,
856   Atmos. Environ., 158, 148-159, https://doi.org/10.1016/j.atmosenv.2017.03.037, 2017.

857   Stokes, R. H. and Robinson, R. A.: Interactions in Aqueous Nonelectrolyte Solutions. I. Solute-
858   Solvent Equilibria, J. Phys. Chem., 70, 2126–2130, DOI: 10.1021/j100879a010, 1966.

859   Su, H., Rose, D., Cheng, Y. F., Gunthe, S. S., Massling, A., Stock, M., Wiedensohler, A., Andreae,
860   M. O., and Pöschl, U.: Hygroscopicity distribution concept for measurement data analysis and
861   modeling of aerosol particle mixing state with regard to hygroscopic growth and CCN
862   activation, Atmos. Chem. Phys., 10, 7489–7503, https://doi.org/10.5194/acp-10-7489-2010,
863   2010.

864   Twomey, S.: The nuclei of natural cloud formation part II: The supersaturation in natural clouds and

the variation of cloud droplet concentration, Geofisica Pura e Applicata, 43, 243–249, DOI: 10.1007/BF01993560, 1959.

Twomey, S.: Pollution and the planetary albedo, Atmos. Environ., 8(12), 1251–1256, https://doi.org/10.1016/0004-6981(74)90004-3, 1974.

Twomey, S.: The influence of pollution on the shortwave albedo of clouds, J. Atmos. Sci., 34(7), 1149–1152, https://doi.org/10.1175/1520-0469(1977)034<1149:TIOPOT>2.0.CO;2, 1977.

van Pinxteren, D., Fomba, K. W., Spindler, G., Müller, K., Poulain, L., Iinuma, Y., Loschau, G., Hausmann, A., and Herrmann, H.: Regional air quality in Leipzig, Germany: detailed source apportionment of size-resolved aerosol particles and compar ison with the year 2000, Faraday Discuss., 189, 291–315, https://doi.org/10.1039/c5fd00228a, 2016.

Varghese, M., Prabha, T. V., Malap, N., Resmi, E. A., Murugavel, P., Safai, P. D., Axisa, D., Pandithurai, G., and Dani, K.: Airborne and ground based CCN spectral characteristics: Inferences from CAIPEEX–2011, Atmos. Environ., 125, 324–336, https://doi.org/10.1016/j.atmosenv.2015.06.041, 2016.

Vepsäläinen, S., Calderón, S. M., Malila, J., and Prisle, N. L.: Comparison of six approaches to predicting droplet activation of surface active aerosol – Part 1: moderately surface active organics, Atmos. Chem. Phys., 22, 2669–2687, https://doi.org/10.5194/acp-22-2669-2022, 2022.

Wang, Y., Wan, Q., Meng, W., Liao, F., Tan, H., and Zhang, R.: Long-term impacts of aerosols on precipitation and lightning over the Pearl River Delta megacity area in China, Atmos. Chem. Phys., 11, 12421–12436, https://doi.org/10.5194/acp-11-12421-2011, 2011.

Wang, Y., Li, Z., Zhang, Y., Du, W., Zhang, F., Tan, H., Xu, H., Fan, T., Jin, X., Fan, X., Dong, Z., Wang, Q., and Sun, Y.: Characterization of aerosol hygroscopicity, mixing state, and CCN activity at a suburban site in the central North China Plain, Atmos. Chem. Phys., 18, 11739–11752, https://doi.org/10.5194/acp-18-11739-2018, 2018a.

Wang, Y., Wu, Z., Ma, N., Wu, Y., Zeng, L., Zhao, C., and Wiedensohler, A.: Statistical analysis and parameterization of the hygroscopic growth of the sub-micrometer urban background aerosol in Beijing, Atmos. Environ., 175, 184–191, https://doi.org/10.1016/j.atmosenv.2017.12.003, 2018b.

Wang, Y., Niu, S., Lv, J., Lu, C., Xu, X., Wang, Y., Ding, J., Zhang, H., Wang, T., and Kang, B.: A new method for distinguishing unactivated particles in cloud condensation nuclei measurements: Implications for aerosol indirect effect evaluation, Geophys. Res. Lett., 46, 14,185–14,194, https://doi.org/10.1029/2019GL085379, 2019.

Wang, Z., Birmili, W., Hamed, A., Wehner, B., Spindler, G., Pei, X., Wu, Z., Cheng, Y., Su, H., and Wiedensohler, A.: Contributions of volatile and nonvolatile compounds (at 300°C) to condensational growth of atmospheric nanoparticles: An assessment based on 8.5 years of observations at the Central Europe background site Melpitz, J. Geophys. Res. Atmos., 122, 485–497, doi:10.1002/2016JD025581, 2017.

Wiedensohler, A.: An approximation of the bipolar charge distribution for particles in the sub-micron size range, J. Aerosol Sci., 19, 387–389, DOI: 10.1016/0021-8502(88)90278-9, 1988.

Wiedensohler, A., Birmili, W., Nowak, A., Sonntag, A., Weinhold, K., Merkel, M., Wehner, B., Tuch, T., Pfeifer, S., Fiebig, M., Fjäraa, A. M., Asmi, E., Sellegri, K., Depuy, R., Venzac, H., Villani, P., Laj, P., Aalto, P., Ogren, J. A., Swietlicki, E., Williams, P., Roldin, P., Quincey, P., Hüglin, C., Fierz-Schmidhauser, R., Gysel, M., Weingartner, E., Riccobono, F., Santos, S., Grüning, C., Faloon, K., Beddows, D., Harrison, R., Monahan, C., Jennings, S. G., O'Dowd, C. D., Marinoni, A., Horn, H.-G., Keck, L., Jiang, J., Scheckman, J., McMurry, P. H., Deng, Z., Zhao, C. S., Moerman, M., Henzing, B., de Leeuw, G., Löschau, G., and Bastian, S.: Mobility particle size spectrometers: harmonization of technical standards and data structure to facilitate high quality long-term observations of atmospheric particle number size distributions, Atmos. Meas. Tech., 5, 657–685, https://doi.org/10.5194/amt-5-657-2012, 2012.

Wiedensohler, A., Wiesner, A., Weinhold, K., Birmili, W., Hermann, M., Merkel, M., Muller, T., Pfeifer, S., Schmidt, A., Tuch, T., Velarde, F., Quincey, P., Seeger, S., and Nowak, A.: Mobility particle size spectrometers: Calibration procedures and measurement uncertainties, Aerosol Sci. Tech., 52, 146–164, https://doi.org/10.1080/02786826.2017.1387229, 2018.

Wu, Z. J., Poulain, L., Birmili, W., Größ, J., Niedermeier, N., Wang, Z. B., Herrmann, H., and Wiedensohler, A.: Some insights into the condensing vapors driving new particle growth to CCN sizes on the basis of hygroscopicity measurements, Atmos. Chem. Phys., 15, 13071–13083, https://doi.org/10.5194/acp-15-13071-2015, 2015.

Wu, Z. J., Zheng, J., Shang, D. J., Du, Z. F., Wu, Y. S., Zeng, L. M., Wiedensohler, A., and Hu, M.: Particle hygroscopicity and its link to chemical composition in the urban atmosphere of Beijing, China, during summertime, Atmos. Chem. Phys., 16, 1123–1138, https://doi.org/10.5194/acp-16-1123-2016, 2016.

Ye, X., Tang, C., Yin, Z., Chen, J., Ma, Z., Kong, L., Yang, X., Gao, W., and Geng, F.: Hygroscopic growth of urban aerosol particles during the 2009 Mirage-Shanghai Campaign, Atmos. Environ., 64, 263–269, https://doi.org/10.1016/j.atmosenv.2012.09.064, 2013.

Zdanovskii, B.: Novyi Metod Rascheta Rastvorimostei Elektrolitovv Mnogokomponentnykh Sistema, Zh. Fiz. Khim+, 22, 1478–1485, 1486–1495, 1948.

Zhang, F., Li, Y., Li, Z., Sun, L., Li, R., Zhao, C., Wang, P., Sun, Y., Liu, X., Li, J., Li, P., Ren, G., and Fan, T.: Aerosol hygroscopicity and cloud condensation nuclei activity during the AC3Exp campaign: implications for cloud condensation nuclei parameterization, Atmos. Chem. Phys., 14, 13423–13437, https://doi.org/10.5194/acp-14-13423-2014, 2014.

Zhang, F., Li, Z., Li, Y., Sun, Y., Wang, Z., Li, P., Sun, L., Wang, P., Cribb, M., Zhao, C., Fan, T., Yang, X., and Wang, Q.: Impacts of organic aerosols and its oxidation level on CCN activity from measurement at a suburban site in China, Atmos. Chem. Phys., 16, 5413–5425, https://doi.org/10.5194/acp-16-5413-2016, 2016.

Zhang, F., Wang, Y., Peng, J., Ren, J., Collins, D., Zhang, R., Sun, Y., Yang, X., and Li, Z.:

941   Uncertainty in predicting CCN activity of aged and primary aerosols, J. Geophys. Res. Atmos.,

942   122(21): 11,723-11,736, https://doi.org/10.1002/2017JD027058, 2017.

943   Zhao, C., Klein, S. A., Xie, S., Liu, X., Boyle, J. S., and Zhang, Y.: Aerosol first indirect effects on

944   non-precipitating low-level liquid cloud properties as simulated by CAM5 at ARM sites,

945   Geophys. Res. Lett., 39, L08806, https://doi.org/10.1029/2012GL051213, 2012.

946   Zhao, C., and Garrett, T. J.: Effects of Arctic haze on surface cloud radiative forcing, Geophys. Res.

947   Lett., 42(2), 557–564, https://dx.doi.org/10.1002/2014GL062015, 2015

948

949
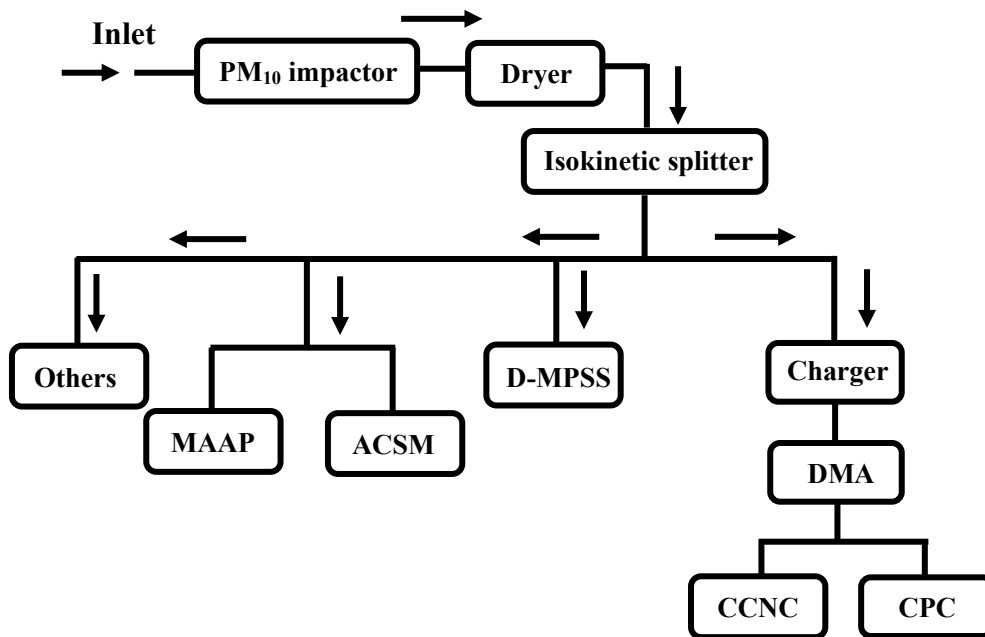
Figure 1. Schematic diagram of the experimental setup. D-MPSS — Dual-mobility particle size

spectrometer, ACSM — aerosol chemical species monitor, MAAP — multi-angle absorption

photometer, DMA — differential mobility analyzer, CPC — condensation particle counter, CCNC

— cloud condensation nuclei counter.

954

955
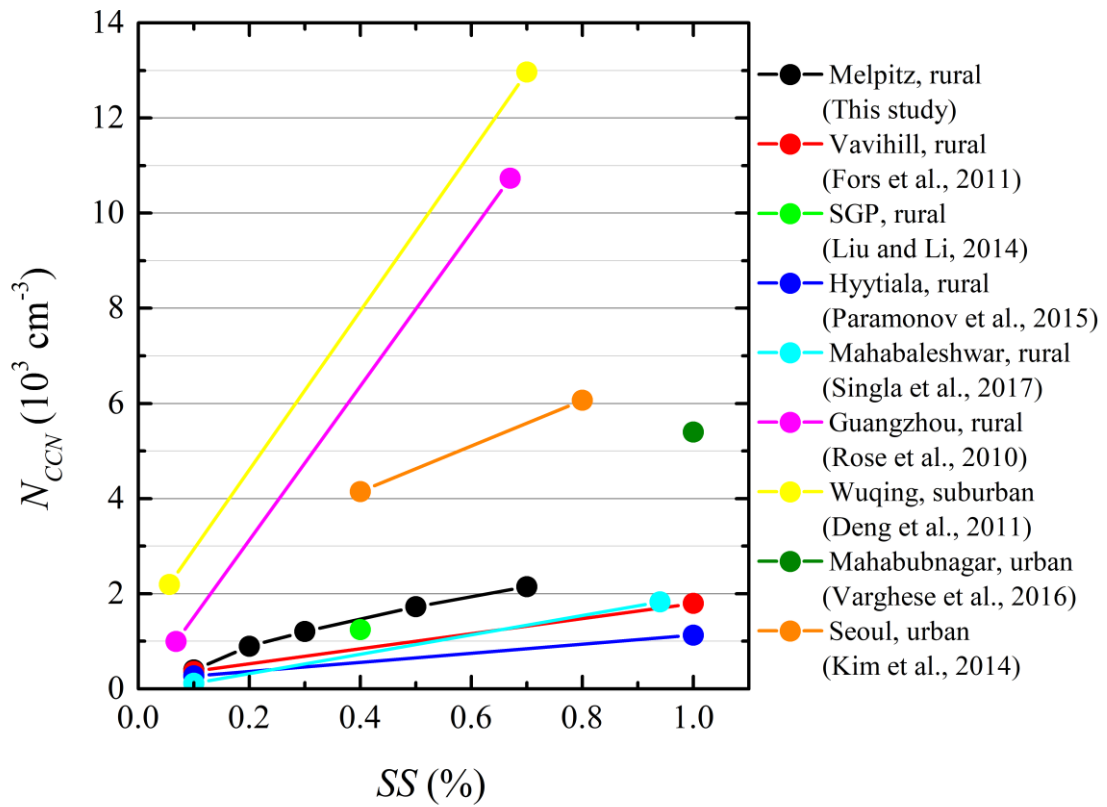
Figure 2. Relationship between CCN number concentration (N_{CCN}) and supersaturation (SS)

957 measured at Melpitz and other stations.

958
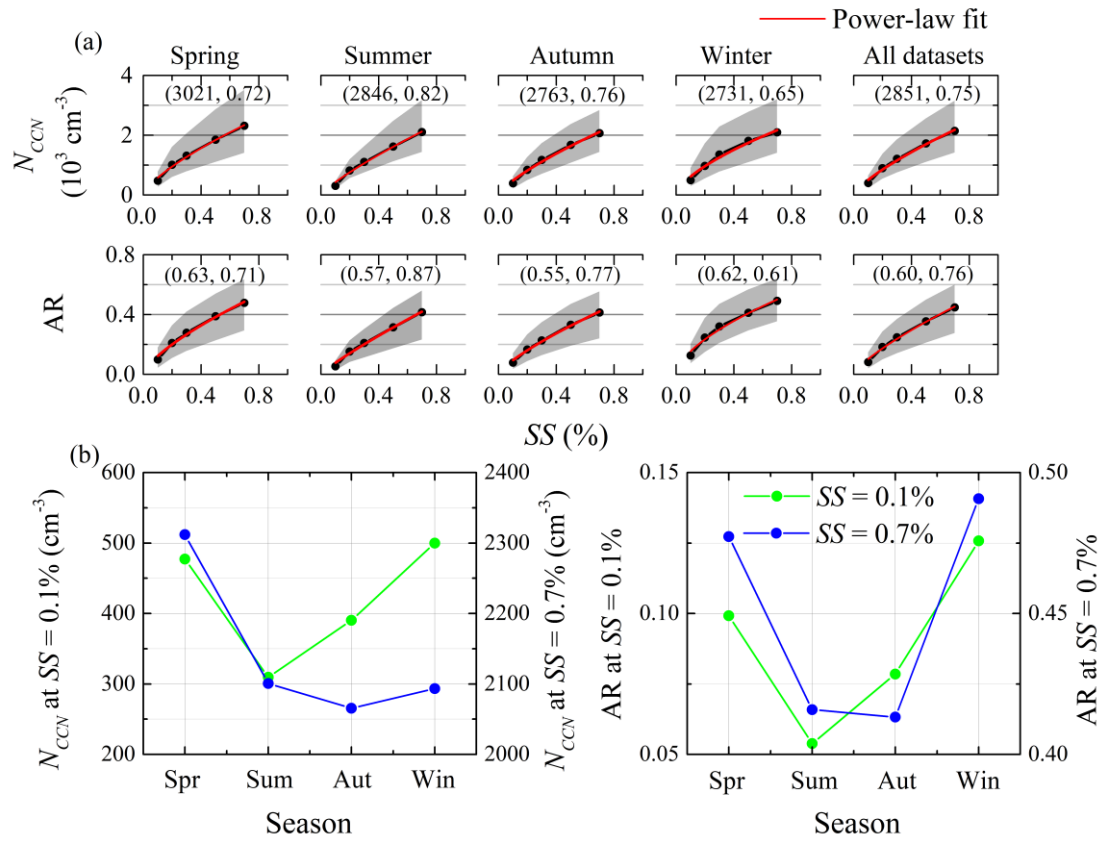
959

960 Figure 3. (a) Relationships between CCN number concentration (N_{CCN}) and supersaturation (SS),

961 and relationship between activation ratios (AR) and SS for different seasons. (b) Seasonal trends of

962 N_{CCN} and AR at SS = 0.1% and 0.7%. Dots represent the median values of N_{CCN} and AR. Shaded

963 areas represent the values in the range from 25th to 75th percent. Red lines are power-law fittings for

964 N_{CCN} (and AR) vs. SS. Two parameters of the fitting results are shown in brackets.

965
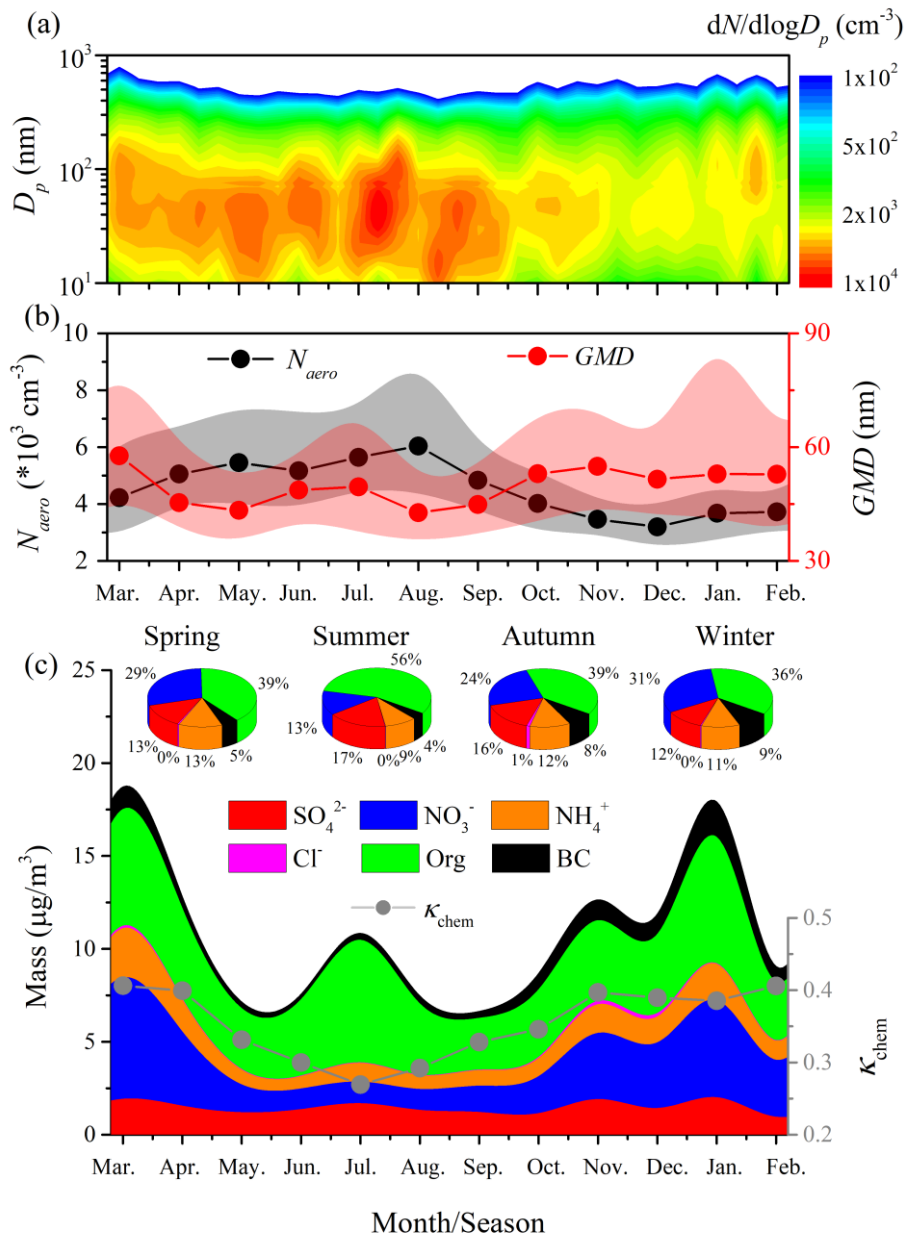
Figure 4. Seasonal variations of (a) aerosol particle number size distribution (dN_{aero}/dlogD_p vs. D_p, D_p is particle diameter), (b) total aerosol number concentration with a D_p range of 10 to 800 nm (N_{aero}) and geometric mean diameter of the particles (GMD), and (c) mass concentration and ratio of each component in aerosol particle with D_p less than 1 μm and the hygroscopicity factor calculated from the chemical composition (κ_{chem}). Dots represent the median values. Shaded areas represent the values in the range from 25th to 75th percent.

973
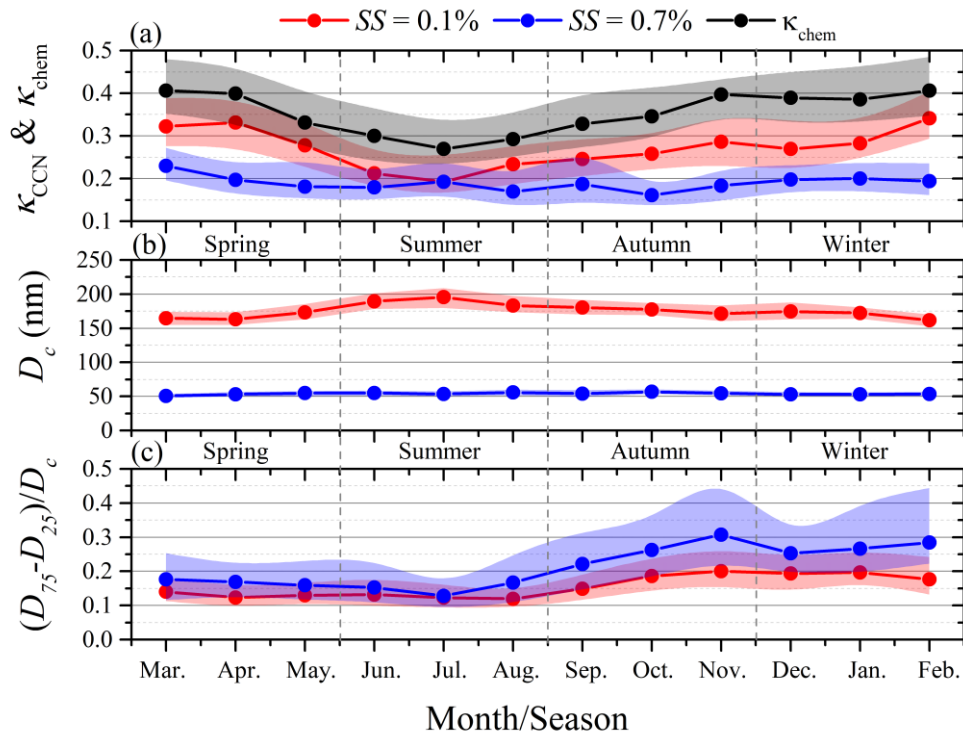
Figure 5. Monthly variations of (a) hygroscopicity factor calculated from monodisperse CCN measurements (κ_{CCN}) at supersaturation (SS) of 0.1% and 0.7%, and hygroscopicity factor calculated from particle chemical composition (κ_{chem}), (b) critical diameter of dry particle for activation (D_c) at SS = 0.1% and 0.7%, and (c) the degree of external mixture (($D_{75} - D_{25})/D_c$) at SS = 0.1% and 0.7%. The definitions of D_{75} and D_{25} are the D_p at which 75% and 25% of the particles are activated at the given SS, respectively. Dots represent the median values. Shaded areas represent the values in the range from 25th to 75th percent.

981
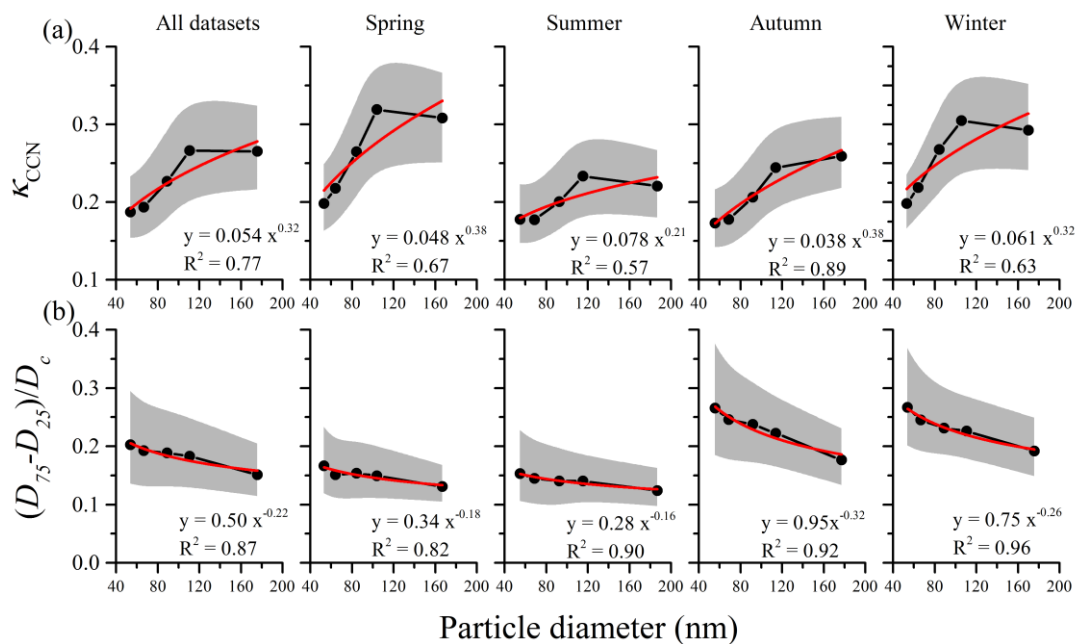
Figure 6. (a) Relationship between the hygroscopicity factor calculated from monodisperse CCN

measurements (κ_{CCN}) and particle diameter (D_p), and (b) degree of external mixture (($D_{75} - D_{25})/D_c$)

vs. D_p at each season. The definitions of D_{75} and D_{25} are the D_p at which 75% and 25% of the

particles are activated at the given SS, respectively. Red lines are power-law fits. Dots represent the

median values. Shaded areas represent the values in the range from 25th to 75th percent.

987
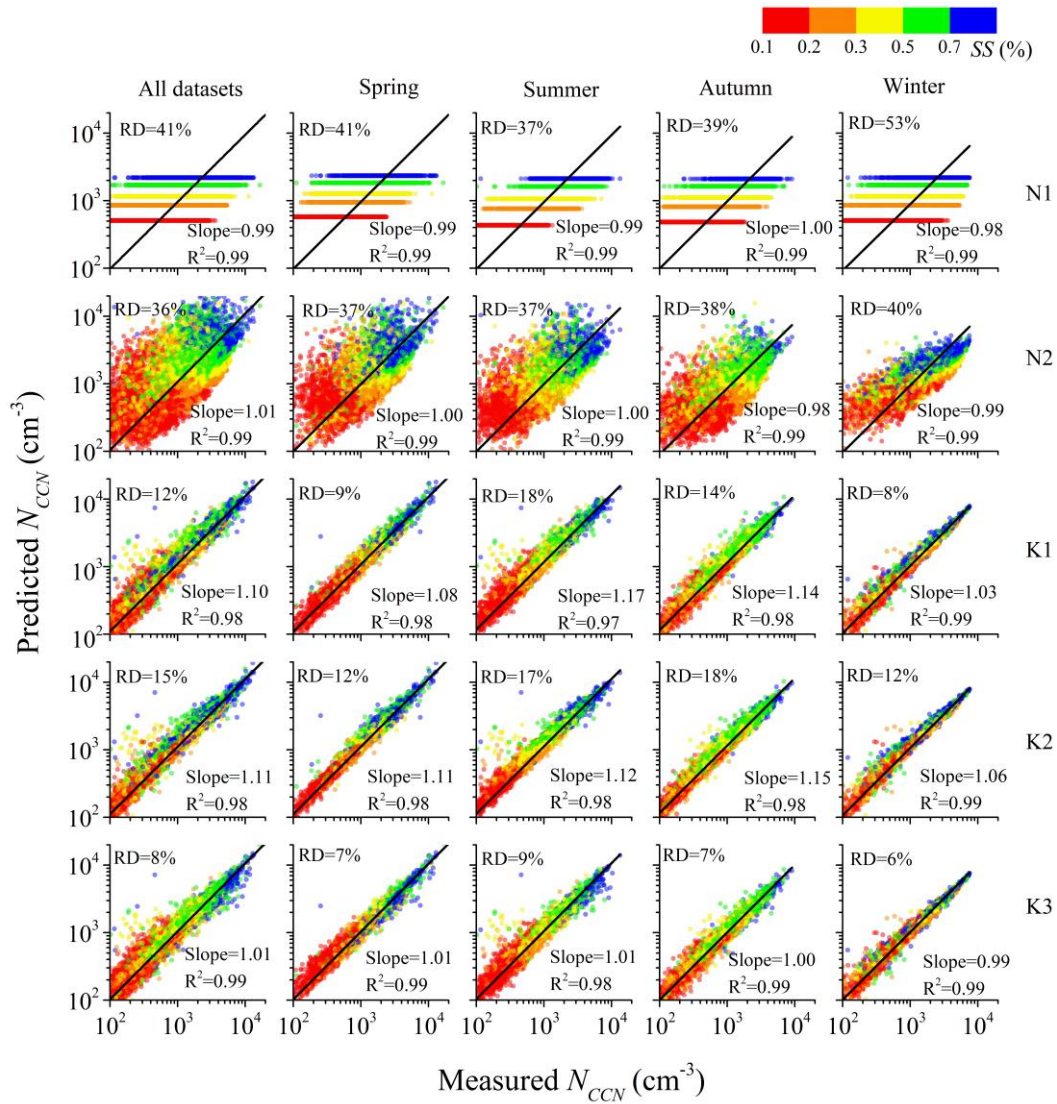
Figure 7. Predicted vs. measured CCN number concentration (N_{CCN}) for different seasons. The Predicted N_{CCN} is calculated from five different schemes with a detailed introduction shown in Table 3. Color bar represents the different supersaturation (SS) conditions. Black lines are the linear fits. The slope and R^2 of the linear regression and the median relative deviation (RD) between the predicted and measured N_{CCN} are shown in each panel. Each row represents the results using the same scheme in different seasons. Each column represents the results using different schemes in the same season.
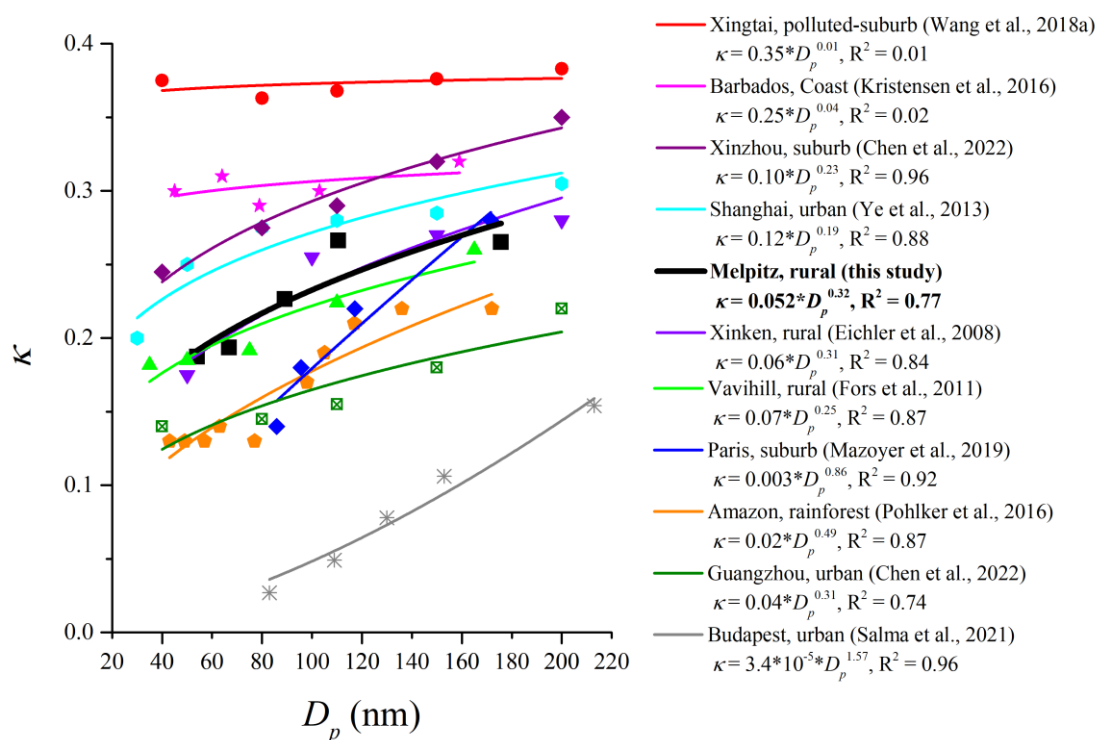
997

998 Figure 8. Relationships between the particle hygroscopicity factor (κ) and diameter (D_p) observed

999 at different stations. Lines are power-law fits of κ vs. D_p.

1000

1001 Table 1. Densities (ρ) and hygroscopicity factor (κ) for each component.

Species	NH_4NO_3	$(NH_4)_2SO_4$	NH_4HSO_4	H_2SO_4	Organics	BC
ρ (kg m^{-3})	1720	1769	1780	1830	1400	1700
κ	0.67	0.61	0.61	0.92	0.1	0

1002

Table2. Seasonal median values of hygroscopicity factor derived from the chemical composition (κ_{chem}), hygroscopicity factor derived from monodisperse CCN measurements (κ_{CCN}), the critical diameter of dry particle for activation (D_c), and the degree of external mixture (($D_{75} - D_{25}$)/D_c) at each supersaturation (SS) condition. The unit of D_c is nm.

Parameters	SS (%)	All datasets	Spring	Summer	Autumn	Winter
κ_{chem}	-	0.30	0.32	0.24	0.31	0.34
κ_{CCN}	0.1	0.27	0.31	0.22	0.26	0.29
	0.2	0.27	0.32	0.23	0.24	0.30
	0.3	0.23	0.26	0.20	0.21	0.27
	0.5	0.19	0.22	0.18	0.18	0.22
	0.7	0.19	0.20	0.18	0.17	0.20
D_c	0.1	176	167	187	177	170
	0.2	111	104	116	114	106
	0.3	89	85	93	92	84
	0.5	67	64	69	69	64
	0.7	54	53	55	55	53
($D_{75} - D_{25}$) /D_c	0.1	0.15	0.13	0.12	0.18	0.19
	0.2	0.18	0.15	0.14	0.22	0.23
	0.3	0.19	0.15	0.14	0.24	0.23
	0.5	0.20	0.15	0.14	0.25	0.25
	0.7	0.20	0.17	0.15	0.27	0.27

1008 Table 3. Introduction of five activation schemes. The meaning of the abbreviation can be found in

1009 Notation list.

Category	Scheme	Introduction
1st category: N_{CCN} - SS or AR - SS empirical fit	N1	N_{CCN} - SS power-law fits shown in Table 3
	N2	Real-time N_{aero} combined with AR - SS power-law fits shown in Table 3
2nd category: Real-time PNSD combined with the parameterized κ	K1	Real-time PNSD combined with a constant κ of 0.3
	K2	Real-time PNSD combined with the real-time bulk κ_{chem}
	K3	Real-time PNSD combined with κ - D_p power-law fits shown in Figure 6a

1010